The Performance of Fluidized Beds, Packed Beds, and Screens as Fuel Cell Electrodes

by

Justin Ruflin

Submitted to the Department of Mechanical Engineering
in Partial Fulfillment of the Requirements for the Degree of
Master of Science in Mechanical Engineering

at the

Massachusetts Institute of Technology

February 2006

Signature of Author.....
Department of Mechanical Engineering
January 25, 2006

Certified by.....
Ernest G. Cravalho
Professor of Mechanical Engineering
Thesis Supervisor

Accepted by.....
Lallit Anand
Chairman, Department Committee of Graduate Students

Fluidized Beds, Packed Beds, and Screens as Fuel Cell Electrodes

by

Justin E. Ruflin

Submitted to the Department of Mechanical Engineering
on January 25, 2006 in partial fulfillment of the
requirements for the Degree of Master of Science in
Mechanical Engineering

ABSTRACT

At present, most fuel cells employ porous gas diffusion (PGD) electrodes. Although much effort has been spent on their development, the performance and cost of PGD electrodes are still major obstacles to the successful commercialization of fuel cells. As a means to bypass the drawbacks associated with PGD electrodes, several researchers have taken an alternative approach to electrode design by considering fluidized bed electrodes (FBEs), a type of flooded electrode that relies on convective rather than diffusive mass transport. Several reviews and past studies claim that FBEs have the potential for reaching high power density at a low cost due to several inherent advantages. However, the results so far of fluidized bed electrodes applied to fuel cells have been poor, and the past studies have not offered effective explanations for the discrepancy between expected and actual performance.

A fluidized bed electrode model has been developed and applied to the data obtained by previous researchers in order to explain the poor performance of these past designs. As points of comparison, models have also been developed to predict the performance of packed bed electrodes and screen electrodes (two other flooded electrode designs). Separate models have been developed to consider both ionic and mass transport. Upper bounds on the performance of all three electrodes have been established, and then compared to the performance of PGD electrodes. The results of the models indicate that the PGD electrodes perform better than the packed bed or screen electrodes by at least a factor of two, unless the flooded electrodes are very short (on the order of millimeters). Both mass transfer and the saturation concentration of oxygen in the electrolyte serve as limitations in the flooded designs. The models also indicate that the two-phase and three-phase FBEs are inferior to the other flooded electrodes. The paper concludes with several recommendations for further work, including methods to boost performance.

Thesis Supervisor: Ernest G. Cravalho

Title: Professor of Mechanical Engineering

1.0 Introduction

Fuel cells have the opportunity to play a large role in future energy conversion systems due to their high efficiency and environmental compatibility, particularly when implemented with renewable energy sources. In addition, their potentially high energy density, particularly with liquid fuels, and continuous operation (no recharging) would be clear advantages in markets where batteries have been unable to keep pace, such as portable electronics (Flipsen, 2005; Yeom, 2005). At present, however, fuel cells are not utilized in any of the potential major markets.

Fuel cells still need to be improved if they are to compete with current energy conversion systems. Specifically, the cells need to be made more robust, the power densities increased, and the costs reduced [1]. All three of these issues can be addressed by the development of better electrodes. The electrode design directly dictates the number and efficiency of reactions taking place on the electrode structure and thus the fuel cell power density. Poisoning, clogging, sealing problems, water management issues, and compatibility with certain fuels are all consequences of the electrode design. The electrodes account for roughly 50% of the fuel cell cost and their supporting structures account for another 30% [2]. If the losses in the electrodes could be decreased, and the cost and complexity of these structures reduced, many of the obstacles to fuel cell commercialization could be diminished if not eliminated.

A large portion of fuel cell research is dedicated to improving the electrodes. However, most studies to date have focused on incremental improvements to current designs. In particular, the majority of low temperature fuel cell work has focused on porous gas diffusion (PGD) electrodes primarily applied to the proton exchange membrane (PEM) fuel cell architecture. Considering the limited scope of this approach, it is not surprising that advancement has been slow. Further progress on the well established designs seems only to be occurring with more difficulty as the potential means to improvement are tried and exhausted.

Several studies have attempted to take a more radical approach to electrode design by considering the application of a very different type of electrode known as a fluidized bed or three-dimensional electrode. Fluidized bed electrodes (FBEs) are considered to have several advantages over porous gas diffusion (PGD) electrodes, the state-of-the-art. Their expected "high rates of heat and mass transfer," large electrode area per unit volume and simple design of the fluidized bed electrode give it the "potential for very high power densities in a very low cost package" [3]. Further, the 3-D structure of the fluidized bed electrode (in contrast to the planar shape of the PGD electrode) is expected to result in scaling advantages [4].

However, attempts to apply fluidized bed electrodes to fuel cells have met with limited success, and the past studies have not offered effective explanations for the discrepancy between expected and actual performance.

The objectives of this thesis are to:

1) Provide the analysis required to explain the results of past research on fluidized bed electrodes.
2) Support or reject the claims on performance made in past papers. Specifically, that fluidized bed electrodes exhibit
    a. high rates of mass transfer,
    b. high surface area per unit volume,
    c. and scaling advantages due to their 3-D structure.
3) Provide an upper bound in performance for typical FBEs.
4) Provide an upper bound for flooded fuel cells in general, of which FBEs are one type of electrode.
5) Introduce several possible methods to improve the performance of FBEs and flooded fuel cells.

2.0 Comparison of Porous Gas Diffusion Electrodes with Fluidized Bed Electrodes

PGD electrodes and FBEs differ significantly in the way in which they fulfill the requirements of a fuel cell electrode. In this section, the function and objectives of electrodes in general are first described. The two electrode types are then introduced along with estimates of their performance; a brief summary of significant FBE research to date is also provided.

2.1 Function of the Fuel Cell Electrode

A fuel cell combines fuel and an oxidizer electrochemically to produce water, electricity, and entropy that must be transported from the cell in the steady state. The total reaction for an alkaline fuel cell running on hydrogen and oxygen gas is

$$H_2 + \frac{1}{2}O_2 = H_2O$$

This chemical reaction is achieved through two electrochemical reactions that occur on catalyst particles that have been deposited on the two fuel cell electrodes (the anode and the cathode). On the anode:

$$H_2 + 2OH^- = 2H_2O + 2e^-$$

While on the cathode:

$$\frac{1}{2}O_2 + H_2O + 2e^- = 2OH^-$$

Electricity is produced directly in the form of the electrons that pass from the anode to the cathode through an external circuit. As is illustrated by the reaction equations, each catalyst particle must be supplied with the reactant gas as well as pathways for incoming/outgoing water, ions, and electrons. If any component is missing, then the catalyst particle is inactive. These catalyst sites that are active and thus comprise the

reaction sites on the electrode are further subject to three major irreversibilities, which reduce power output:

1. The *activation overpotential* due to the kinetic characteristics of the catalyst material.
2. The *ohmic overpotential* due to the finite ionic mobility of the electrolyte resulting from the processes of diffusion and migration of the ions from one electrode to the other.
3. The *concentration overpotential* due to the finite rate at which reactants can get to the catalyst sites.

These irreversibilities are referred to as overpotentials because each represents a loss that shows up explicitly as a decrease in the electrode potential (voltage). Since the power output of the cell is the product of this electrode voltage and the current of electrons passing from one electrode to the other through the load, a reduced voltage due to these overpotentials results in lower power output.

The activation overpotential is due primarily to the catalyst material, but the latter two overpotentials can be directly related to the design of the electrodes. The challenge in electrode design is to try to keep the latter two irreversibilities as low as possible while at the same time creating as many active catalyst sites as possible.

2.2 Brief Description of PGD Electrodes

PGD electrodes achieve the mentioned requirements by employing a very thin and highly porous electrode structure. This electrode structure contacts the electrolyte on one side and the reacting gas on the other, as shown in Figure 1; the catalyst material is contained in the pores of the electrode. Both electrolyte and gas seep into the porous structure from their respective sides. The interface in the pores where the electrolyte and gas meet is governed by capillary action; this interface is the site where the reactions take place, and thus ideally where the majority of catalyst resides.

The porous structure is useful for two reasons. First, the pores create a larger surface area than would otherwise be available to a planar electrode. Second, and maybe more importantly, the capillary action in the pores acts to thin the layer of electrolyte covering the electrode surface and catalyst reaction sites. To actually react, the gas must dissolve into the electrolyte at the gas-electrolyte interface and then diffuse through the electrolyte to the reaction sites. The diffusion of the gas in the electrolyte is slow enough that even a thin layer of electrolyte severely hinders transport. If the electrode was smooth, even with agitation, the thinness of the electrolyte film would be on the order of 10 to 100 micrometers [5]. Using models discussed later in this thesis, particularly equation (18), it can be shown that a 10 micrometer film of 6 Molar KOH electrolyte at 80 °C on a flat electrode would restrict the current to about 0.8 mA/cm^2, which is less than a fraction of a percent of the current produced by a typical PGD electrode. In the porous structure of a PGD electrode, the gas and electrolyte interface forms a meniscus, the shape of which is governed by surface tension. If the pore were simply a cylindrical hole, the meniscus might look similar to a hemisphere, as shown in Figure 1. The electrolyte layer on the

pore wall thins along the sides of the meniscus, eventually vanishing to zero at the meniscus rim. The thinness of the diffusion layer near the meniscus rim provides a low resistance to gas diffusion and thus improves mass transport. The optimal region is near but not at the very end of the meniscus since at the end of the meniscus there is no electrolyte for ions to diffuse through which creates too high of an ion diffusion resistance.

Catalyst sites far from the meniscus, immersed in the electrolyte-filled pore, are essentially inactive since they are cut off from the dissolved gas. Likewise, any sites outside of the meniscus, exposed only to gas are also inactive. The active sites reside only at essentially the three-phase interface consisting of the solid carbon of the electrode, the liquid electrolyte, and the gas. If the catalyst is not near the three-phase interface or the catalyst is not connected electronically to the electrode, the catalyst is not active and no appreciable reactions occur. Consequently, "even for a best 'architecture' of the catalyst layer, electrochemically-active surface fractions of Pt [the catalyst] comprise ~ 40% of the total Pt surface" [6].

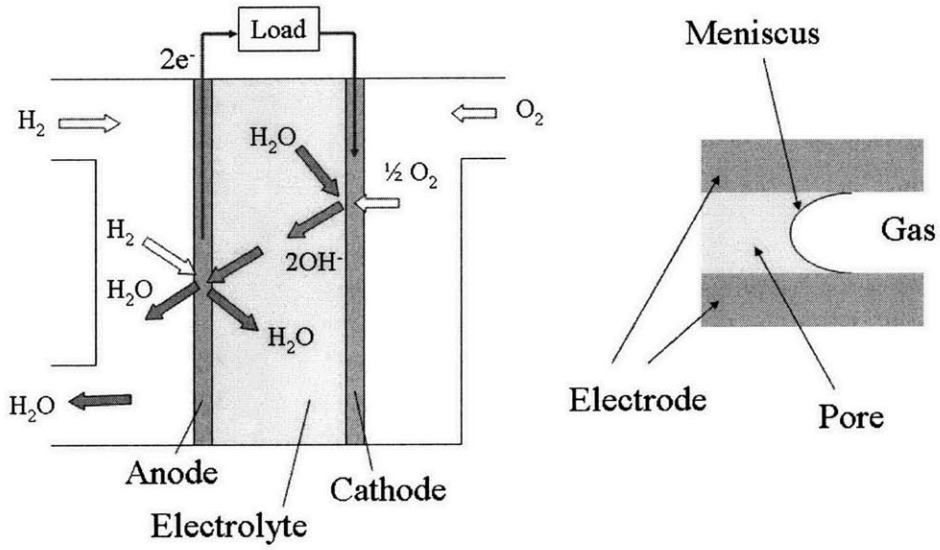

Figure 1: Left-hand side of figure is a schematic of the general configuration and reactions of an alkaline electrolyte fuel cell. The right-hand side shows a simplified depiction of the porous electrode structure, highlighting the meniscus formed at the interface of the electrolyte and reacting gas.

The PGD electrode structure has a significant impact on the electrode performance. In a PGD electrode sufficient space must be assigned to each transport process. For example, if too much catalyst is deposited or the electrode is not porous enough, not enough space will be left for gas and ion diffusion, and the electrode performance will consequently suffer. If the pore sizes are highly variable, the location of the meniscus in each pore will also be highly variable, and performance will again suffer. The smaller pores will tend to flood with electrolyte, the larger pores will tend to dry out, and a significant portion of the catalyst sites in the electrode will consequently be inactive. The balance of the competing requirements is a difficult and delicate optimization process and contributes

significantly to the high costs of PGD electrodes [7]. Despite the development efforts that have gone into PGD electrode design, the electrodes are still not optimized, largely because "most of the known 'technologically-friendly' fabrication procedures [used for manufacture and optimization] reveal hardly any degree of precision and reproducibility" [6].

2.3 Brief Description of 2-Phase and 3-Phase Fluidized Bed Electrodes

In contrast to the PGD electrode, the fluidized bed electrode relies on convection for mass transport, rather than diffusion, and a "flooded" electrode architecture. The structure of a two-phase fluidized bed electrode consists primarily of a bed of catalyst-coated particles through which an electrolyte is passed. The drag induced on the particles by the flow of electrolyte at sufficiently high velocities causes the particles to "fluidize," i.e. to become mobile but not entrained, in the flow of the electrolyte. The transport of reactants to and from the surface of the electrode is facilitated by this flow of electrolyte around the particles. The structure is considered flooded because the entire electrode is essentially immersed in electrolyte; there are no dry regions as in a PGD electrode. A three-phase fluidized bed electrode is similar in design to a two-phase fluidized bed except that both the reacting gas and the electrolyte are bubbled through the bed.

The components of a fluidized bed electrode are shown in Figure 2. In addition to the electrode particles, a fluidized bed electrode consists also of a distributor and current collector. The distributor is the component responsible for creating a uniform flow of both the electrolyte and/or gas through the bed while the current collector acts as the electrical connection for the bed. The current collector and distributor could be separate pieces of hardware in the bed, or a single component could serve both functions. For example, a metal porous plate that supports the particles of the bed could act as both the current collector and the gas/electrolyte distributor.

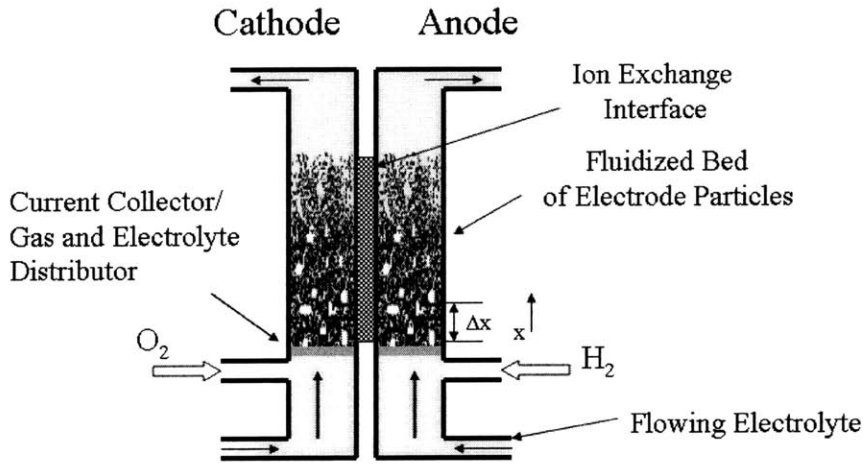

Figure 2: General configuration of a fuel cell employing fluidized bed electrodes.

The rate of mass transfer in the fluidized bed is expected to be rather high as a consequence of the combined effects of the agitation of the bed due to the flow of electrolyte (and gas if bubbled through the bed), the high rates of convective transport

due to the flow of the electrolyte, and the high surface area to volume ratio of the particles. Since the bed is dynamic, the careful creation of static three-phase interfaces is no longer a concern. Unlike a PGD electrode, the fluidized bed electrode does not have portions of the electrode volume dedicated to just ion or gas or electron transport or catalyst; thus the balancing requirements responsible for the complexities of operation and high cost of PGD electrodes are no longer an issue. Furthermore, in a fluidized bed electrode, water management, a major issue in a PGD electrode, is also no longer a concern since it is no longer necessary to ensure that pores in the electrode do not dry out or flood. Also, the "ease of construction, maintenance and operation [of the fluidized bed electrode] makes it attractive" [4]. The manufacture of the electrode is trivial compared to the PGD electrode, and the optimization of performance of the fluidized bed electrode is much easier.

2.4 Lower Bound for Typical PGD Electrode Performance

Data on typical fuel cells employing PGD electrodes are readily available from either manufacturers or the literature. The task of this section is to convert the available data into a form that is comparable to the FBE performance data in later sections. The performance parameter that we would ideally like to use is power per unit volume of the complete fuel cell. However, the fluidized bed electrode data are only for half-cells, so only the volume of the cathode is known. Guessing the volume of the anode and supporting structures for a fuel cell employing fluidized bed electrodes adds significant uncertainty. To avoid introducing this uncertainty into the calculations, all data for both fuel cells employing PGD electrodes and fuel cells employing FBEs are instead converted to total power output per unit volume of the cathode, rather than total power output per unit volume of the complete fuel cell.

We can find the total power output per volume of the cathodes in a fuel cell employing PGD electrodes using commercial fuel cell data. The manufacturer's data give dimensions and total power output for either the fuel cell stack alone, which is the aggregate of all the individual fuel cells, or the complete fuel cell system, which consists of the fuel cell stack plus the ancillary devices. Half the fuel cell stack or approximately half the fuel cell system consists of volume dedicated to the cathodes alone. Thus if the total volume of the stack or system is divided by two, then the approximate volume of the cathodes is determined. The total power output divided by the total volume occupied by the cathodes is then the power density per unit volume of the cathodes. This data are given in Table 1 for two PEM fuel cells manufactured by Ballard Power Systems and one alkaline fuel cell (AFC) manufactured by Astris Energi. The alkaline fuel cell is a stack only, where the area of each electrode used to calculate the total volume is only the active area. If the supporting structure of the stack was considered as well, the power density would be lower. The total volume referred to in Table 1 is the total volume of the system, so the cathode volume is approximately half of that listed. Note that the alkaline fuel cell is a lab test cell, so not as much development has gone into this stack as the commercial PEM fuel cells. This lack of development could be the primary cause of the discrepancy between the power densities of the two types. Note that the Mark 9 SSL is a stack only, while the Mark 902 is a complete system. As expected, the stack alone has a higher power compared to the complete system, which includes the ancillary devices as well.

As an alternative method to determining the power density per unit volume of PGD cathodes, the data in the literature can be considered. Data in the literature consists of current and power output per unit nominal (instead of real) surface area of typical (not necessarily state-of-the-art) electrodes. Electrodes are typically less than a fraction of a millimeter in thickness, so even though the gas-electrolyte interface in the electrode is three-dimensional, the electrode is a two-dimensional structure on the scale of the fuel cell. Thus, data is given in terms of area rather than volume since the thickness of the electrode is almost negligible compared to the size of the fuel cell anyways. The variability of the electrode thickness is thus removed from the performance calculation.

To obtain the current density and power density per unit volume for a typical PGD electrode, the current density and power density per unit area is divided by the thickness of half a typical single fuel cell. The thickness of the fuel cell is primarily due to the bipolar plates, which act as a gas manifold and the electrical connection between different fuel cells in a fuel cell stack. Bipolar plates for PEM fuel cells that were 0.3 cm in thickness were created in reference [8]. The work of reference [9] focused on creating bipolar plates by an injection molding process; bipolar plates of 0.25 – 0.4 cm in thickness were obtained.

If a bipolar plate size of 0.4 cm is chosen as a reasonable upper bound in thickness, then half of this plate size is the thickness dedicated to each electrode. The assembly consisting of the electrodes and the separation layer of electrolyte is typically less than 1 mm in thickness. So then a reasonable value for half of a fuel cell is around 2 mm.

The current density and corresponding voltage for several PEM and alkaline fuel cells are given in Table 2; the data is a sampling of the data in the review of alkaline fuel cell technology in reference [3]. The power output (voltage multiplied by current) of the fuel cell at the given operating points is also given in Table 2. If the values of current density and power density per unit area are divided by a thickness of 2 mm, then a power density and current density per unit volume are obtained; these values are also listed in Table 2. All data are for fuel cells running on hydrogen and air at 1 atm.

Table 1: Performance of Fuel Cell Stacks or Systems Employing PGD Electrodes

Electrolyte, Ref.	Model	Total Vol., (cm^3)	*i*, (A)	Volt., (V)	Power, (kW)	Power, (W/ cm^3)	Oxygen Source
PEM [10]	Mark9 SSL	14866	300	70	21	2.82	Air at 1 atm
PEM [11]	Mark 902	75469	300	284	85	2.26	Air at 1 atm
AFC [12]	MC250	18000	---	---	2.4	0.26	Air at 1 atm

Table 2: Performance of Fuel Cells Employing PGD Electrodes [3]

Electrolyte	*i*, (A/ cm^2)	Volt., (V)	Power, (W/ cm^2)	*i*, (A/ cm^3)	Power, (W/ cm^3)	Oxygen Source
Alkaline	0.45	0.7	0.315	2.3	1.6	Air at 1 atm
Alkaline	0.29	0.7	0.2	1.5	1.0	Air at 1 atm
PEM	0.50	0.6	0.3	2.5	1.5	Air at 1 atm
PEM	0.45	0.6	0.27	2.3	1.4	Air at 1 atm

2.5 Prior Research and Performance of Fluidized Bed Electrodes

Only a few studies on fluidized bed electrodes in fuel cells have been conducted. Berent et al. in 1971 [13] studied alkaline fluidized bed electrodes composed of ballotini glass beads coated with silver, platinum, or platinum-ruthenium alloy catalysts. In their study, "extreme difficulty was encountered in stabilizing a 3-phase fluidized bed" [13]. For this reason, they studied only two-phase beds using liquid oxidants, such as hydrogen peroxide, and liquid fuels. These studies included measurements of temperature, bead size, fuel type, and oxidizer type on electrode performance. It is worth noting that they also used a metal probe to study bed deactivation and metal potential distribution in the bed. They found that the potential in a fluidized bed cathode became more positive relative to the feeder, starting about half way up the bed (max difference was about 0.1 V for a current of 200 mA/cm^2) for both 0% and 16.6% fluidization (extent of fluidization at least up to 16.6% thus did not affect the result). They also tested a fluidized bed anode running on methanol for bed deactivaton. They found that the beads disconnected electronically from the current collector, and parts of the electrode were thus deactivated as fluidization increased. The bed began to deactivate after 10% fluidization. Half the bed was considered deactivated at about 20% fluidization.

Fleischmann, Oldfield, and Porter in 1971 investigated a solid/liquid fluidized bed of ballotini glass beads coated with silver catalyst as a cathode for alkaline fuel cells [14]. The electrolyte consisted of 1 molar KOH that was saturated with oxygen before it entered the bed. They presented two models. The first of these related an effective mass-diffusion layer thickness to the limiting current while the other correlated cell performance at low currents with both the resistivity of the particles in the bed and the reaction kinetics. Of particular interest is the model for low currents, which was used to calculate the specific resistivity of the particles at different locations in the bed. They found that "variations in voidage throughout the bed, together with entrance effects close to the distributor, cause a continuous increase in [the effective specific resistivity of the discontinuous metal phase] in the direction of fluid flow" [14].

In 1990, Tanaka et al. studied a complete fuel cell consisting of two three-phase fluidized bed electrodes separated by a glass filter [15]. These electrodes were fluidized by the bubbling gas only; the electrolyte was not circulated through the bed but remained stationary, and only gas was fed into the electrode. Activated carbon impregnated with silver was used as the catalyst (minus 300 mesh fraction). In contrast to the previous studies, Tanaka and co-workers used cylindrical current collectors on the walls of the bed

that they found to have improved bed contact compared to plate current collectors. Tanaka et al. performed longevity tests and found that for a given current output of the cell "the potential was stable and did not vary over 150 [hours]" [15].

Matsuno and co-workers have studied both molten carbonate fuel cell anodes and alkaline fuel cell cathodes. Only the alkaline electrodes will be reviewed here. In 1996, Matsuno et al. [7] studied a three-phase fluidized bed cathode where both the electrolyte and the gas were passed through the electrode bed. Both sintered silver beads (1-3 mm in diameter) and porous Raney silver particles (0.6 mm diameter) were tested. Matsuno et al. also measured bed polarity using the same technique as in reference [13]. Matsuno et al. [7] measured a uniform potential in the bed regardless of the extent of fluidization and bed expansion for levels of fluidization up to about 10 %. This is contrary to the results of both reference [13] and reference [14] and can probably be attributed to the very high conductivity of silver particles compared to glass beads. However, Matsuno et al. [7] did measure a "rapid fall-off of potential near the current collector due to poor electrical contact between the current collector and the electrode particles."

In 1997, Matsuno et al. [4] improved the contact between the bed and the current collector by dimpling the plate that served as the collector. They tested both Raney silver particles and platinum-coated Raney-silver particles (0.6 mm diameter). The platinum coated particles produced improved results, as would be expected since platinum is a better catalyst than silver (though more expensive) for oxygen reduction in alkaline fuel cells.

A summary of the performance of several of the fluidized bed electrodes running on oxygen in the discussed papers is presented in Table 3. All data are for cathodes only. The level of fluidization in the electrode is listed, unless it was not given in the reference. Overvoltage is given rather than voltage since these are single electrodes. The length of the electrode was considered to be the length of the bed; the actual test cells were usually much longer. For the data from reference [15], a bed height was not clear, so the height of the current collectors was used instead. The best power is also given; this value was determined by subtracting the overvoltage from the ideal operating voltage of a hydrogen-oxygen fuel cell (1.23 V) and then multiplying this value by the current density. Again, note that the power densities and current densities in Table 3 are based on the volume of the cathode alone rather than the volume of a complete fuel cell in order to avoid the complication of guessing the volumes of the anode and other structures.

Table 3: Fluidized Bed Electrode Performance

Ref.	Bed Area, (cm^2)	Bed Ht., (cm)	I, (A/cm^3)	Over-Volt(V)	Best P., (W/cm^3)	Electrolyte Conc.	Fluid-iztn.	Oxidizer
[4]	20.4	2.7	0.015	0.23	0.015	6 M	N/G	O_2 1 atm
[14]	7	1	0.080	0.5	0.058	1 M	10 %	O_2 1 atm
[15]	4.9	5	0.012	0.23	0.012	6 M	N/G	O_2 1 atm

The results given in Table 3 are clearly poor compared to the performance of the typical PGD electrodes in Tables 1 and 2. Note that the performance of the FBEs in Table 3 would only get worse if air were used as the oxidizer, as was the case for the fuel cells in Tables 1 and 2. Current scales directly with the saturation concentration of oxygen in the electrolyte, and the concentration of oxygen scales directly with the partial pressure of the oxygen in the gas phase. The performance of the PGD electrodes in Tables 1 and 2 is consequently expected to increase by a factor of at least 3 and up to 5 times if the fuel cells were run on pure O_2, as was the case in Table 3.

The PGD electrodes seem clearly superior, yet the investigators in references [3], [4], and [7] in particular indicate that fluidized bed electrodes have the potential for high performance. In order to help clarify these results and the expectations of performance, we now introduce a model describing the performance of a fluidized bed electrode.

3.0 Development of the Model to Predict the Maximum Current

References [4] and [14] provide a substantial amount of data that can be used to reveal more detail regarding the performance of the fluidized bed electrode. As an aide to the proper interpretation of the results of references [4] and [14], we have formulated a simple phenomenological model. Despite its simplicity, this model allows us to form several important conclusions about fluidized bed electrodes.

Specifically, we are interested in the maximum possible mass transfer rate to the electrode surface for reaction, which can then be converted to the limiting current of a particular electrode design. For our purposes here, let us examine a one-dimensional bed of unit cross-sectional area in the y-z plane normal to the x-axis. Consider a slice of the bed of thickness Δx parallel to the y-z plane as shown in Figure 2. During the time interval Δt, the difference between the number of moles of oxygen leaving the bed, $\Delta n_{x+\Delta x}$, and the number entering the bed, Δn_x, is equal in magnitude and opposite in sign to the number of moles of oxygen reacted within the slice.

$$\Delta n_{x+\Delta x} - \Delta n_x = -\Delta n_r \tag{1}$$

If we divide equation (1) through by Δt and take the limit as the time interval shrinks to zero, equation (1) becomes the rate at which oxygen is reacted within the slice, dn_r/dt. Then

$$\lim_{\Delta t \to 0} \frac{\Delta n_{x+\Delta x} - \Delta n_x}{\Delta t} = \dot{n}_{x+\Delta x} - \dot{n}_x = \lim_{\Delta t \to 0}\left(-\frac{\Delta n_r}{\Delta t}\right) = -\frac{dn_r}{dt} \tag{2}$$

The molar flux $\dot{n}_{x+\Delta x}$ can also be written in terms of $\dot{V}$, the volumetric flow rate of the incompressible electrolyte with oxygen concentration $C_{x+\Delta x}$ (moles/volume):

$$\dot{n}_{x+\Delta x} = \dot{V} C_{x+\Delta x} \tag{3}$$

Equation (2) can then be written

$$-\frac{dn_r}{dt} = \dot{V}\left(C_{x+\Delta x} - C_x\right) \tag{4}$$

In the limit $\Delta x \to dx$, the slice becomes infinitesimal in thickness with an infinitesimal change in concentration, and equation (4) becomes

$$-\frac{dn_r}{dt} = \dot{V}dC \tag{5}$$

The rate of reaction of oxygen per unit of reactive surface in the bed is given by

$$\frac{1}{Adx}\frac{dn_r}{dt} = k_m\left(C - C_s\right) \tag{6}$$

where k_m is the mass transfer coefficient, A is the reactive surface area per unit length, C is the bulk concentration of oxygen at position x, and C_s is the concentration of oxygen at the reactant surface. The maximum possible mass transfer rate occurs when the surface concentration of oxygen, C_s, is zero. Thus, setting C_s equal to zero and combining equations (5) and (6), we have

$$\dot{V}dC = -k_m ACdx \tag{7}$$

Integrating the resulting differential equation (7) over the length of the bed L gives an expression for the outlet oxygen concentration in terms of the inlet oxygen concentration:

$$C_{out} = C_{in}\cdot\exp\left(\frac{-k_m AL}{\dot{V}}\right) = C_{in}\cdot\exp\left(\frac{-k_m A_S}{\dot{V}}\right) \tag{8}$$

where A_S is the total surface area of the bed and $\dot{V}$ is the volumetric flow rate of electrolyte.

For a two-phase liquid-solid fluidized bed, the mass transfer coefficient is given by [16]:

$$Sh_p = \left(0.23 \to 0.31\right) Ar^{1/3} Sc^{0.4\to 0.33} \tag{9}$$

where Sh_p is the Sherwood number, Ar is the Archimedes number, and Sc is the Schmidt number. The Sherwood number is defined as

$$Sh_p = \frac{k_m d_p}{D_{O_2}} \tag{10}$$

where D_{O_2} is the diffusion coefficient of oxygen and d_p is the particle diameter. The Archimedes number is defined as

$$Ar = \frac{d_p^3 \left(\rho_p - \rho_f\right) \rho_f g}{\mu^2} \tag{11}$$

where ρ_p is the particle density, ρ_f is the fluid density, g is the gravitational constant, and μ is the viscosity of the electrolyte. The Schmidt number is defined as

$$Sc = \frac{\mu}{\rho_f D_{O_2}} \tag{12}$$

Note that the expression for the mass transfer coefficient in equation (9) is independent of the Reynolds number (which is a dimensionless expression for velocity); this is due to the fact that an increase in superficial velocity also increases bed expansion. The expanded bed decreases the number of particles per unit volume in the bed, which opens up more space for the flowing electrolyte. The ratio of the velocity in the bed to the superficial velocity consequently decreases in accordance with mass conservation. Thus a higher superficial velocity is offset almost exactly by the effect of bed expansion, and the mass transfer coefficient consequently remains independent of the Reynolds number.

The difference between the lower and upper bounds in equation (9) is not large. Choosing the lower bound of equation (9), we get

$$k_m = 0.31 D_{O_2}^{2/3} \left[\frac{\left(\rho_p - \rho_f\right) g}{\mu} \right]^{1/3} \tag{13}$$

For the case of a 3-phase fluidized bed, equation (13) gives a lower bound to the mass transfer coefficient [17]. This is due to the fact that an increase in the superficial velocity also increases bed expansion.

The current produced by the oxygen consumed in the bed is given as

$$i = zF\left(C_{in} - C_{out}\right)\dot{V} \tag{14}$$

where z is the number of electrons an oxygen molecule contributes to the reaction, ideally four, and F is Faraday's constant. Combining equations (8), (13), and (14), we obtain the desired expression for the maximum current output of the electrode if we assume that C_{in} is the saturation concentration of oxygen in the electrolyte, C_{sat}, which, in turn, depends on electrolyte concentration, temperature, and the partial pressure of oxygen.

$$i_{\lim} = zF\dot{V}C_{sat}\left\{1 - \exp\left(-\frac{0.31 A_S D_{O_2}^{2/3}}{\dot{V}} \left[\frac{\left(\rho_p - \rho_f\right) g}{\mu} \right]^{1/3} \right)\right\} \tag{15}$$

As in equation (15), A_s is the total surface area, which can be found by multiplying the specific surface area of the particles by the volume of the bed. The superficial specific surface area, a_s, of perfectly smooth particles in a bed is determined from the definition

$$a_s = \frac{\text{Particle Surface Area}}{\text{Volume Occupied}} = \frac{4 \cdot \pi \cdot r^2}{(2 \cdot r)^3} = \frac{\pi}{d_p} \tag{16}$$

where r is the particle radius and d_p is the particle diameter. The parameter a_s is derived in equation (16) assuming the particles are stacked directly on top of each other. Thus a_s is a lower limit for the specific surface area since the particles would actually arrange themselves into a denser stacking configuration, and the volume occupied would be less than that used in equation (16).

4.0 The Model Applied to the Two-Phase Bed of Reference [14]

The model is first applied to the two-phase bed of reference [14]. The results of the model should be reasonable since the conditions in this bed were close to those assumed in the model: the fluidized bed was run as a two-phase bed only and the electrolyte was presaturated with oxygen before it entered the bed.

4.1 Bed and Electrolyte Parameters

The fluidized bed of reference [14] was 3 cm in diameter and 1 cm high. Ballotini glass beads of 452-520 micrometers, coated with silver by the Brashear process, were used as the particles in this bed. The properties of the particles are given in Table 4. Note in Table 4 that the superficial surface area, a_s, which was calculated using equation (16), is close in value to the wetted and dry specific surface area values quoted from the paper. The particles thus have minimal surface roughness.

The properties of the 1 M KOH electrolyte at 25 C are given in Table 5.

Table 4: Physical Properties of the Silver Coated Glass Beads

Particle Size, d_p (mm)	Density, ρ_p (g/cm^3)	Spec. Surf. Area, a_m, wetted (cm^{-1})	Spec. Surf. Area, a_m, dry (cm^{-1})	Superficial Spec. Area, a_s (cm^{-1})
0.452 - 0.520	2.6	65	72	69.5 – 60.4

Table 5: Properties of the 1 M KOH Electrolyte at 25 C

Diffusion Coefficient, D_{O_2} (cm^2/s)	O_2 Sat. Concentration, C_{sat} (mol/cm^3)	Density, ρ_f (g/cm^3)	Viscosity, μ (Pa·s)
$1.42 \cdot 10^{-5}$	$0.80 \cdot 10^{-6}$	1.05	$1.01 \cdot 10^{-3}$

4.2 Results of the Model

Using the data in Tables 4 and 5, the only unknowns in equation (15) are then i_{lim}, $\dot{V}$, and A_S. We can solve for A_S in equation (15) by using the measured values of i_{lim} and U taken from reference [14]. The volume flux U is the superficial velocity of the electrolyte, which is equal to the volumetric flow rate, $\dot{V}$, divided by the cross-sectional area of the bed.

Note also that in equation (15), A_S is the total surface area. Then to compare to the specific surface area, a_m, given in reference [14], we divide A_S by the total volume of the bed. The results of these calculations, the calculated specific surface areas a_c for the three superficial electrolyte velocities, are given in Table 6.

Alternatively, we could ignore A_S by assuming that it is very large. In this case, all the oxygen is consumed and the exponential term in equation (15) goes to zero. Then a maximum possible current output, i_{max}, can be determined by assuming that all the oxygen pre-saturated in the electrolyte is consumed. The values of i_{max} are also shown in Table 6.

Table 6: Results of the Model

Velocity, U (mm/s)	i_{lim}, (A)	i_{lim}, (A/cm^3)	a_m, (cm^{-1})	a_c, (cm^{-1})	a_c / a_m	i_{max}, (A)	Fluidization
5.32	0.48	0.069	65	30	46.2 %	1.15	5%
8.85	0.60	0.085	65	34	52.3 %	1.91	10%
14.2	0.66	0.094	65	35	53.8 %	3.07	25%

4.3 Accuracy of the Model

The primary output of the model in Table 6 is the calculated surface area, a_c. As can be seen from the results, the value of a_c is relatively constant for all velocities, but is only about 50% of the expected surface area. Thus according to the model, the electrode appears to be only using half of its available surface area. Several factors could contribute to this result.

One explanation could be that parts of the bed are inactive. Since the particles are fluidized, each particle is not necessarily in electrical contact with the bed 100% of the time. The surface area of those disconnected particles does not contribute to the output of the electrode, so the overall active surface area of the bed decreases which in turn decreases the specific surface area.

Another explanation could be that the voltage within the bed is not constant. Even if the particles are connected most of the time, electrical resistance associated with particle-to-particle contact could cause a voltage polarization of the bed. The reaction at the particles is ultimately driven by the metal potential of the electrode. As the potential is driven more negative, the reaction is forced to occur faster, and the concentration of the reactant at the surface of the electrode drops. Ultimately the surface concentration is driven to zero, and the mass transport to the electrode can increase no further; this condition is the

limiting current, and is responsible for the concentration overpotential described in Section 2.1.

If the metal potential within the bed varies, then the metal potential in certain regions of the bed may not be negative enough to drive the surface concentration of oxygen to zero. If this is the case, then setting C_s equal to zero and writing equation (7) is no longer correct. The surface concentration on the particles with a higher potential will be greater than zero, the concentration gradient driving mass transport to these particles will be less than the maximum, and a lower than expected current will result. Indeed, reference [13] tested the local potential versus the potential of the current collector for a fluidized bed cathode consisting of silver coated beads, which is the same type of bed particle used in reference [14]. The measurements revealed that a potential gradient existed in the bed regardless of the extent of fluidization.

The value of z could also be a cause for the model calculating a lower than expected surface area. The number of electrons that the oxygen molecule actually contributes depends on the reaction pathway. For an efficient catalyst such as platinum, the oxygen reacts to form primarily hydroxyl ions and the value of z approaches 4, which is what the model assumes. However, for a silver catalyst in an electrolyte of low concentration at a relatively low temperature, as in reference [14], the oxygen-oxygen bond in the O_2 molecule may not always be broken and z is expected to be less. If the reaction produces mostly hydrogen peroxide, the value of z can be as low as 2.

The accuracy of the model is not excellent, but given that the error is constant, the results of the model seem reasonable. By ignoring voltage variations in the bed, and assuming an upper limit for z, the model predicts the upper limit for the performance of the fluidized bed electrode.

4.4 Conclusions

1. Mass flux into the electrode limits performance.
One of the primary obstacles to suitable performance evident from the results in Table 6 is the mass transport of reactant oxygen into the electrode. Even if all the oxygen transported into the electrode reacts, the electrode still produces very little current, as is clear from the values of i_{max} given in Table 6. From Tables 1 and 2, a PGD electrode the size of the electrode in reference [14] would produce a current output of at least 7 A. If the PGD electrode were run on pure O_2, the electrode current should be greater than 30 A or about 10 times the greatest value of i_{max} given in Table 6. The amount of oxygen carried into the fluidized bed electrode by the electrolyte is clearly insufficient to produce currents comparable to those produced by the PGD electrodes.

The current output of the electrode can be written in essentially the same form as equation (15) but without inserting equation (13) for k_m.

$$i_{\lim} = zF\dot{V}C_{sat}\left\{1-\exp\left(\frac{-k_m A_S}{\dot{V}}\right)\right\} \tag{17}$$

Any electrode for which the electrolyte is charged with oxidant before it enters the electrode, and then the electrolyte flows through the electrode, is governed by equation (17). What is interesting about equation (17) is that it shows that regardless of the electrode surface area, or the magnitude of the mass transport, the ultimate performance is still limited by the amount of reacting mass that initially flows into the electrode. This is different from the equation for mass transfer for the PGD electrode, which can be written as

$$i_{max} = zFA_{S_{PGD}} \frac{D_{O_2}}{\delta}\left(C_{sat} - C_s\right) \tag{18}$$

where $A_{S_{PGD}}$ is the active surface area in the PGD electrode and δ is a characteristic thickness of the electrolyte diffusion layer in the electrode. Since a typical PGD electrode is always exposed to a large reservoir of oxygen gas, the C_{sat} term in equation (18) remains essentially constant across the entire electrode. Consequently, the surface area, $A_{S_{PGD}}$, the effective mass transfer coefficient, D_{O_2} / δ, and C_{sat} are all equally important in producing the maximum possible current.

2. The fluidized bed electrode does not exhibit high rates of mass transfer compared to a PGD electrode.

One of the claims made in past work was that fluidized bed electrodes have high rates of mass transfer. To test this assumption, we can directly compare the FBE performance to the PGD electrode performance given by equation (18).

Assume the electrolyte could remain saturated as it flowed through the fluidized bed electrode, regardless of how much oxygen reacted. Equation (17) could then be written as

$$i_{max\_sat} = zFA_S k_m \left(C_{sat} - C_s\right) \tag{19}$$

Equation (19) is an upper bound, since C_{sat} will actually drop as the electrolyte travels through the bed, which, in turn, will reduce the mass transfer. Equation (19) is in the same form as equation (18). For a given set of electrolyte properties, equations (18) and (19) differ only by the surface area times the mass transfer coefficient for either the FBE or PGD electrode (either $A_S k_m$ or $A_{S_{PGD}} D_{O_2} / \delta$).

For the fluidized bed in reference [14], if we use a surface area of 65/cm, the maximum current with a saturated electrolyte according to equation (19) would be i_{max_sat} = 1.33 A. As a comparison, a PGD electrode of the same size of the fluidized bed in reference [14] with a power density of about 1 A/cm^3, the lowest value in Table 2, produces a current of 7 A. Thus, the maximum current of the fluidized bed electrode is no more than 1/5th the current of an air breathing PGD electrode of the same size. As before, if the PGD electrode was run using pure O_2, the maximum current of the fluidized bed electrode would be no more than 1/20th of the PGD electrode. The product of the surface area and the mass transfer coefficient for the fluidized bed electrode, $A_S k_m$, is less than the

corresponding product for the PGD electrode, $A_{S_{PGD}} D_{O_2} / \delta$. Therefore, the mass transfer of the fluidized bed electrode is inferior to that of the PGD electrode.

If performance of the fluidized bed electrode is going to be improved, C_{sat} and/or $\dot{V}$ must be increased, and $A_S k_m$ must be maintained at a large enough value that a significant amount of the incoming oxidant is then able to react.

5.0 Extension of the Model to the 3-Phase Bed of Reference [4]

One method of increasing C_{sat} is by bubbling the oxygen directly through the bed to create a three-phase fluidized bed electrode. In this case, the model breaks down, since the replenishment of the oxygen in the electrolyte is not considered. If the model is applied in spite of this limitation, the difference between the expected and actual performance will partly be a result of the bubbling.

The other interesting step that was taken in reference [4] is that the particles used were Raney silver, which has a surface area that is orders of magnitude greater than the geometrical area of the spherical particles. These particles were then coated with platinum, which appeared to increase the surface area slightly further.

5.1 Bed and Electrolyte Parameters

The fluidized bed used in reference [4] was 5.1 cm in diameter and 2.7 cm high. The specifications of the platinum coated Raney particles used in this bed are given in Table 7 [4]. The properties of the 25 wt% KOH electrolyte at 60 C are given in Table 8 (D_{O_2} and C_{sat} are approximated from 80 C data) [18, 19]. The authors in reference [14] explicitly state that the electrolyte was presaturated before it entered the bed. In contrast, reference [4] did not actually specify saturation, so the actual value of C_{sat} could be potentially less than the value given in Table 8.

Table 7: Physical Properties of the Platinum Coated Raney Silver Particles

Particle Size, d_p (mm)	Density, ρ_p (g/cm^3)	Specific Surface Area, a_m (cm^{-1})	Superficial Spec. Area, a_s (cm^{-1})
0.6	4.8	92300	52.4

Table 8: Properties of the 25 wt % KOH Electrolyte at 60 C

Viscosity, μ (Pa·s)	Density, ρ_f (g/cm^3)	Diffusion Coefficient, D_{O_2} (cm^2/s)	O_2 Sat. Concentration, C_{sat} (mol/cm^3)
$1.05 \cdot 10^{-3}$	1.23	$2.0 \cdot 10^{-5}$	$0.104 \cdot 10^{-6}$

5.2 Results of the Model

Note the data from reference [4] only include tests of three-phase beds. The presence of the gas phase should only improve performance [16, 17]. The results of equation (15), the calculated specific surface areas a_c for the three superficial electrolyte velocities, are given in Table 9. Since the model presented here is for a two-phase bed, we use only the data sets with the lowest gas velocity (2.9 mm/s).

As was done in section 4, a maximum possible current output, i_{max}, can be determined by assuming that all the oxygen pre-saturated in the electrolyte is consumed. The values of i_{max} are also given in Table 9.

Table 9: Results of the Model

Velocity, U (mm/s)	i_{lim}, (A)	a_m (cm^{-1})	a_c (cm^{-1})	a_c / a_m	a_c / a_s	$i_{max,}$ (A)
2.9	0.19	92300	10.8	0.012 %	21%	0.24
8	0.30	92300	11.3	0.012 %	22%	0.65
14.5	0.78	92300	35.9	0.039 %	69%	1.19

5.3 Conclusions

1. The surface porosity does not improve performance.

One of the clearest results of the model is the ratio of calculated to measured surface area, a_c / a_m, in Table 9. The fact that the surface area being used is only a fraction of a percent of the Raney surface area indicates that the majority of the area of the Raney particles is inactive. The percent of the geometric surface area that appears to be active is even less than that found for the fluidized bed in Section 4, except for the highest velocity in Table 9.

The reason that the porous surface area is not utilized is a consequence of the poor mass transport in the fluidized bed. Consider the simplified schematic of an electrode particle as shown in Figure 3. As reactions take place on the particle surface, the concentration of oxygen at the particle surface decreases relative to the oxygen concentration of the bulk electrolyte. This decrease in concentration at the surface causes a concentration gradient to form in the electrolyte directly surrounding the particle; this concentration gradient is shown in the upper right corner of Figure 3. The concentration boundary layer, represented by the dashed line labeled Surface 1, is a measure of how far into the bulk electrolyte the concentration gradient extends. Outside of the boundary layer, the gradient is small and the oxygen concentration approaches that of the oxygen concentration in the bulk electrolyte, labeled C_{bulk} in Figure 3. The dashed line labeled Surface 2 denotes the smooth spherical surface area directly above the porous electrode particle. If we assume the concentration at Surface 2 is zero, then the driving force for mass transfer (the concentration difference) is at a maximum between Surfaces 1 and 2 for a given C_{bulk} and mass transfer coefficient. This rate of mass transfer is the limiting rate of the electrode. Note that the amount of surface area below Surface 2 is not considered in determining this rate. The mass transport to Surface 2 is independent of the internal surface area of the porous particle. Thus, if the mass transfer between Surfaces 1 and 2 is poor, then the performance of the electrode will be poor regardless of the internal area. This is the case

in Table 9; the fact that not even all of the nominal surface area is being used indicates that this choking effect is occurring.

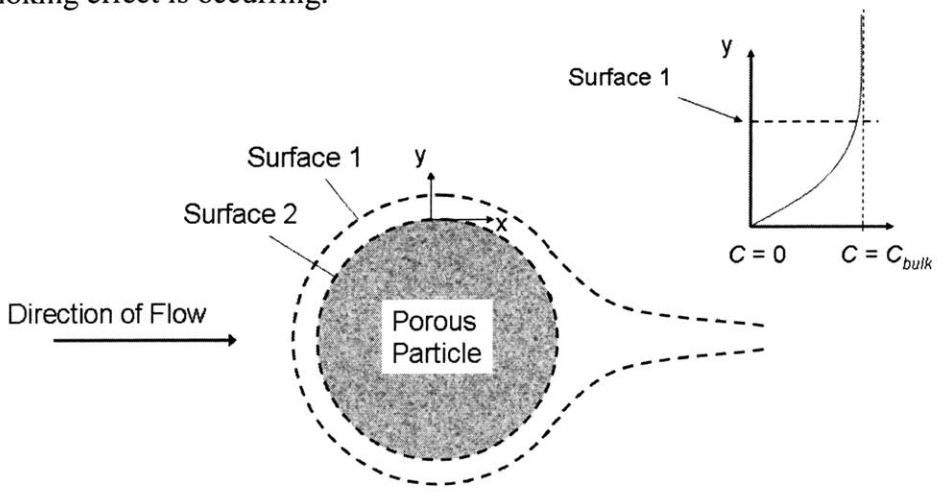

Figure 3: Two surfaces of different concentrations around a porous particle. The concentration profile of oxygen within the boundary layer is shown in the diagram in the upper right. Surface 1 represents the concentration boundary layer. Surface 2 denotes the smooth spherical surface representing the superficial surface of the particle.

The porous particles are actually reducing performance rather than increasing it. From equation (15), we note that greater current output could be achieved if the particles were solid instead of porous. Solid silver particles increase the mass transfer coefficient by 40% over porous ones of the same diameter due to their greater density (refer to equation (13)). Denser particles would also require a higher electrolyte velocity to fluidize, which would improve performance by carrying in more reactant oxygen.

2. Bubbling does not keep the electrolyte saturated with oxygen.
The gaseous oxygen is incapable of keeping the electrolyte saturated as it flows through the bed. In reference [4], the authors state that "the mass transfer resistance of oxygen gas [dissolving] into the liquid phase becomes negligible at high liquid velocity compared to that of dissolved oxygen at the electrode surface." However, the present model indicates that this is not the case. For instance, assume that the particles have a specific surface area of 36/cm, which is the highest calculated value in Table 9 and thus a reasonable estimate of the active area. If equation (13) holds, then according to equation (19) the current that would be produced by an electrode immersed in a saturated electrolyte would still be 60 % higher than the highest measured current in Table 9. If the expected surface area of 52.4/cm given in Table 7 was assumed instead, the current would increase the highest value in Table 7 by 140%. Thus the fluidized bed electrode is not producing current sufficient to indicate that the electrolyte is saturated.

Granted, the data in Table 9 is for a low gas velocity (2.9 mm/s), so one might guess that a higher gas velocity would maintain the electrolyte concentration closer to saturation. If however the gas velocity is increased from 2.9 mm/s to 12 mm/s, the electrode performance only improves by about 7% according to the data in reference [4]. Mass transfer resistance at the electrode surface is substantial (as discussed in Section 5.3);

however, the resistance to dissolving oxygen into the electrolyte is similarly large. Thus the bubbling of oxygen is not sufficient to keep the electrolyte saturated.

3. The distributor design probably hinders performance.
The maximum value of a_c given in Table 9 is even smaller than the expected superficial surface area a_s noted in Table 7. This indicates that even if the particles were perfectly smooth, some area still does not seem to be used. Part of the discrepancy may be due to the distributor design. The holes through which the electrolyte passes in the plate distributor of reference [4] have a total area of only 1/100th the area of the distributor, so the electrolyte probably enters the bed initially in the form of jets. It is likely, then, that particles distant from the holes, but near the collector, are in stagnant oxygen-depleted regions and are thus ineffective.

4. The correlation for k_m probably does not hold at low fluid velocities.
It is noted that the values of a_c for liquid velocities of 2.9 mm/s and 8 mm/s seem almost too small compared with a_s to be attributed solely to the gas distributor design. The gas distributor design also does not necessarily explain why there is a sudden jump in performance from 8mm/s to 14.5 mm/s. It is possible that these low values of a_c may be due partly to a mass transfer coefficient that is smaller than expected.

The minimum fluidization velocity, U_{mf}, which is the electrolyte velocity required just to fluidize the bed of particles in a two-phase bed, is calculated according to the correlation [16]:

$$\frac{d_p \cdot U_{mf} \cdot \rho_f}{\mu} = \left[(25.7)^2 + 0.037 \cdot \frac{d_p^3 \cdot \rho_f \cdot (\rho_p - \rho_f) \cdot g}{\mu^2} \right]^{1/2} - 25.7 \qquad (20)$$

For smooth particles that are the same diameter as those described in Table 7, the minimum fluidization velocity according to equation (20) is at least 8 mm/s. The particles in Table 7 however are porous, and porous particles tend to need a higher velocity for the same level of fluidization as smooth particles [20]. Thus the mass transfer coefficient for a fluidized bed given by equation (13) probably holds for a velocity of 14.5 mm/s, but may not for 2.9 mm/s and 8 mm/s. A value of the mass transfer coefficient that is smaller than that predicted by equation (13) would explain the very low calculated surface area, a_c, at the two lower velocities. Assuming that the model predicts correctly the 14.5 mm/s data, we note that a_c / a_m is greater for this bed than the 2-phase bed evaluated in Section 4. The increase in utilized surface area could be due to the gas phase replenishing the electrolyte, or the value of z being higher due to the platinum catalyst. The increase could also be due to the fact that the particles used in the bed in reference [4] were composed primarily of silver metal coated with platinum rather than glass coated with silver as in reference [14]. The higher conductivity of the primarily silver particles in reference [4] might have resulted in a lower ohmic resistance in the bed, and thus an increase in utilized surface area. The value of the utilized surface area could have been even higher if a better distributor had been used.

6.0 The Effect of Superficial Velocity

From the data in both references [4] and [14], it is clear that as the electrolyte velocity increases, the current produced by the electrode increases as well. This increase in performance with velocity is not due to a higher rate of mass transport, as is evident from equation (13). In a well-behaved fluidized bed electrode, the surface area and the mass transfer coefficient should not change with velocity. The performance improvement is due to the fact as the velocity increases, less of the oxygen carried into the electrode has time to react, and thus the local oxygen concentration at each point in the bed remains closer to saturation. This is evident in equation (8), where as the volumetric flowrate increases, the concentration of oxygen that leaves a given electrode approaches the concentration that entered the electrode, which is the saturation concentration. The closer the oxygen concentration is to saturation at any point in the bed, the higher will be the concentration gradient driving mass transport to the electrode surface, and thus the greater the current flux at that point. Thus a higher velocity improves performance by maintaining the oxygen concentration closer to saturation.

However, a higher electrolyte velocity also causes the bed to expand. As the expansion, or level of fluidization, increases, the particles become less and less often in contact with the current collector of the electrode. The reduced frequency of contact between the particles and the electrical connection of the bed increases the ohmic resistance of the electrode, and can even lead to deactivation of portions of the bed. This ohmic resistance was seen in the voltage/current plots of reference [14] where as the fluidization level increased, the electrode had to be run at more negative potentials just to reach the same current, presumably due to the increasing bed deactivation and polarization of the electrode. Thus for a given particle size, as the velocity and fluidization increase, the performance will not increase indefinitely. Eventually bed deactivation and polarization will outweigh the benefits of a higher velocity, and performance will decrease.

If the particles are increased in size, their weight to drag ratio will increase, allowing them to resist entrainment and tolerate greater electrolyte velocities for a given level of fluidization. However, their surface area to volume ratio will decrease, resulting in a lower specific surface area for the bed. There thus exists an optimum particle diameter for a given set of conditions that will optimize the power output of the electrode. Using the model derived in Section 3.0 and an appropriate equation for the electrolyte velocity, the following section seeks to determine this optimum for various conditions.

6.1 The Velocity Equation

To find the optimum particle diameter for a given set of bed conditions, the optimum velocity for each diameter must be predicted. The velocity through the bed depends in general on the level of fluidization, the particle properties, and the fluid properties.

The level of fluidization can be expressed as

$$\chi = \frac{L_{bed} - L_{bed\_mf}}{L_{bed\_mf}} \tag{21}$$

where L_{bed_mf} is the length of the bed at minimum fluidization and L_{bed} is the length of the bed at a fluidization of χ. Note that the height of the bed when the electrolyte velocity is zero is not necessarily L_{bed_mf}. A static bed will expand as the velocity is increased from zero even if minimum fluidization has not been achieved. The condition that identifies the point of minimum fluidization is the fact that the pressure drop across the bed ceases to change after the minimum fluidization velocity is reached. The best way to find the point of minimum fluidization is to fully fluidize the bed and then slowly decrease the velocity while monitoring the pressure drop across the bed. The minimum fluidization velocity corresponds to the point at which the pressure drop across the bed just begins to decrease. The length of the bed at this velocity is L_{bed_mf}.

In a fluidized bed the volume of the particles is fixed, and can be expressed as [16]

$$L_{bed} A_c (1-\varepsilon) = \text{Packing Volume} = \text{Constant} \tag{22}$$

where A_c is the cross section of the bed perpendicular to the flow and ε is the voidage, or void fraction, of the bed. The voidage is defined as

$$\varepsilon = \frac{\text{Bed Volume - Packing Volume}}{\text{Bed Volume}} \tag{23}$$

where the packing volume is the volume of the material that composes the bed (the total volume of the particles) [21]. The total volume of the particles is always less than the volume of a packed bed of particles, so $0 \le \varepsilon \le 1$.

Since the volume of the particles is fixed, if the length of the bed and voidage of the bed at the minimum fluidization velocity are known, then the length of the bed at any voidage can be determined by rearranging equation (22) as

$$L_{bed}(1-\varepsilon) = L_{bed\_mf}(1-\varepsilon_{mf}) \tag{24}$$

where ε_{mf} is the voidage at minimum fluidization.

Experiment has shown that when the logarithm of the superficial velocity of the fluid entering the bed is plotted against the logarithm of the voidage in a fluidized bed, a straight line with a slope of n is obtained [16]. This relationship can be expressed by the Richardson-Zaki equation as [16]

$$U = U_0 \left(\frac{\varepsilon}{\varepsilon_0} \right)^n \tag{25}$$

where U_0 is the free-settling velocity of the particles, ε_0 is the voidage at the free settling velocity, which is equal to one, and n is a constant dependent on the particle size and density and the fluid properties. The constant n can be determined by solving the equation [16]:

$$\frac{4.8-n}{n-2.4}=0.043(Ar)^{0.57} \tag{26}$$

where the term in parentheses on the right side is the Archimedes number given by equation (11).

Equations (21) and (24) can be combined to solve for the ratio in equation (25):

$$\frac{\varepsilon}{\varepsilon_0}=\frac{1-\frac{1}{1+\chi}\left(1-\varepsilon_{mf}\right)}{\varepsilon_0} \tag{27}$$

U_0 is determined by the empirical correlation by Turton and Clark (1987) [16]:

$$\mathrm{Re}_0=\frac{d_p U_0 \rho}{\mu}=(Ar)^{1/3}\left[\left(\frac{18}{Ar^{2/3}}\right)^{0.824}+\left(\frac{0.321}{Ar^{1/3}}\right)^{0.412}\right]^{-1.214} \tag{28}$$

Solving for n in equation (27) and substituting this value and equation (26) into equation (25), one obtains

$$U=U_0\left[\frac{\left(\chi+\varepsilon_{mf}\right)}{\varepsilon_0\left(1+\chi\right)}\right]^{\frac{4.8+2.4\cdot\left(0.043(Ar)^{0.57}\right)}{0.043(Ar)^{0.57}+1}} \tag{29}$$

where U_0 is determined from equation (28) and $\varepsilon_0 = 1$ by definition.

6.2 Test of the Velocity Equation

Equation (29) can be plotted for the values of the fluidized bed parameters used in reference [14]. These parameters are referred to as the base conditions, and are listed again in Table 10. Equation (29) is plotted as a function of fluidization in Figure 4. The velocity as a function of fluidization for the base conditions is plotted as a solid line. The second line is a variation on the base conditions to indicate the sensitivity of the results. The velocities and corresponding fluidization levels for the three data points in Table 6 are also plotted in Figure 4.

Table 10: Base Conditions

Voidage, ε_{mf}	Particle Diameter, d_p (mm)	Particle Density, ρ_p (g/cm^3)	Fluid Density, ρ_f (g/cm^3)	Viscosity, μ (Pa·s)
0.42	0.48	2.6	1.23	$1.05 \cdot 10^{-3}$

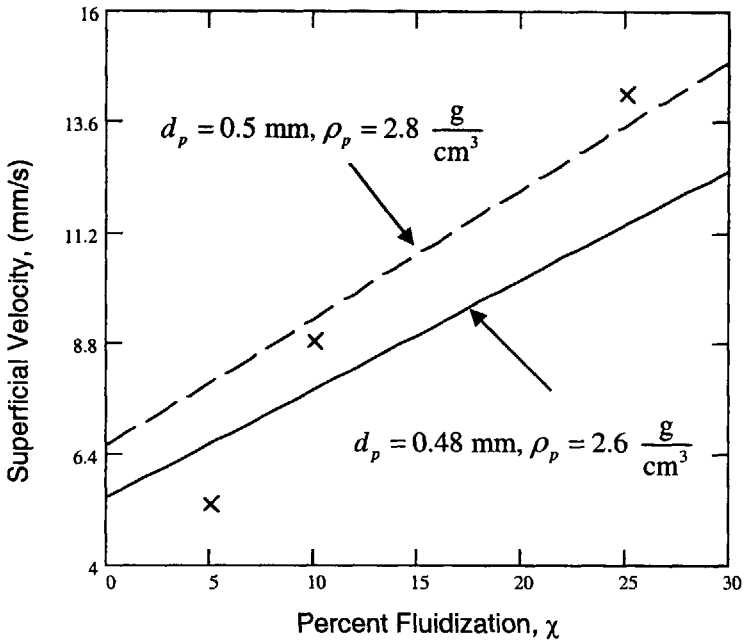

Figure 4: Superficial velocity required to reach a given level of fluidization of the bed for two different sets of particle diameter and density. The 3 data points in Table 6 are also plotted.

As is clear from Figure 4, the data points from Table 6 are predicted by equation (29) and the base conditions in Table 10 within ± 25%, but do show significant scatter. There are only 3 points in Table 6, so there is not much data to compare to the model. The quality of the measurements of the fluidization level in reference [14] is also questionable. If $\log(U)$ is plotted versus $\log(\varepsilon)$ the resulting line is not straight, as expected by equation (25). Equation (25) should hold until very high voidage values (at least $\varepsilon = 0.8$).

Part of the scatter may be due to the fact that the particles are not monosized spheres as the model assumes, but vary over a significant range (0.452 – 0.52 mm). The density of the particles was also guessed, using a general value for glass. Assuming instead a density for glass of 2.8 g/cm^3 and a diameter of 0.5 mm instead of 0.48 mm, the predictions of the model can be improved for the data at 10% and 25% fluidization, as is shown in Figure 4. The 25% fluidization point can be predicted by the model if the diameter is increased to 0.52 mm, which is the size of the largest particles in the bed.

The scatter in Figure 4 may also be due to experimental error. The method of fluidization measurement is not described in reference [14]. Unless the measurement method was very precise, determining the level of fluidization for a 1 cm tall bed composed of spheres of various sizes was probably difficult, especially at the lowest levels of fluidization. The 5% fluidization data point in Figure 4 happens to be the worst fit to the model given by equation (29).

Regardless of the uncertainties and variations in the input data, equation (29) does predict the general trends. In the optimization of the fluidized bed performance in Section 6.3 and Section 7, equation (29) will be used unmodified, but with the understanding that an error of up to 25% could be possible.

6.3 The Influence of Bed Parameters on Performance

Rewriting equation (17) in terms of velocity instead of volumetric flow rate, one obtains

$$i_{\lim} = zFA_c UC_{sat}\left\{1-\exp\left(\frac{-\pi k_m L_{bed}}{d_p U}\right)\right\} \tag{30}$$

where U is given by equation (29), k_m is given by equation (13), and a_s has been replaced by equation (16). Equation (30) then gives an expression for the limiting current as a function of particle diameter, level of fluidization, the minimum fluidization voidage, the length of the bed, the density of the particles, and the fluid properties.

Using the base conditions in Table 10, assuming a length of the bed of 1 cm, and a bed area of 7 cm^2 (the same as in reference[14]), equation (30) can be plotted for various levels of fluidization as shown in Figure 5. Alternatively, holding the level of fluidization constant at 15%, Figure 6 is a plot of the results of equation (30) for different values of density. Finally, equation (30) is plotted for various lengths in Figure 7, keeping the density and fluidization level constant at 2.6 g/cm^3 and 15%, respectively.

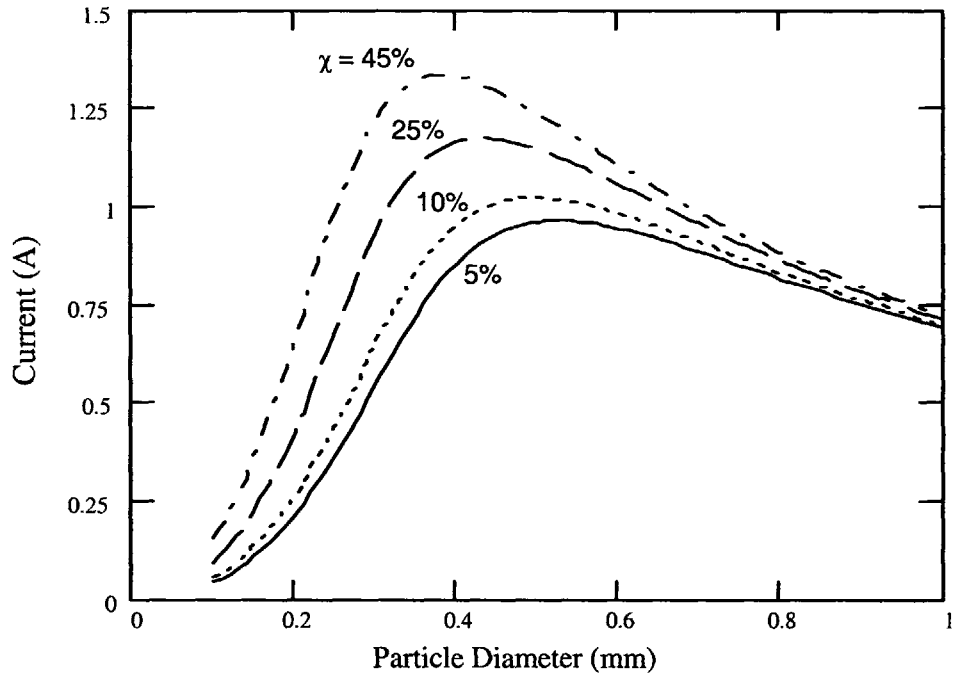

Figure 5: Effect of the level of fluidization on current output as a function of particle diameter. The bed and electrolyte parameters are those given in Table 5 and Table 10. The bed is 1 cm long, and has a cross-sectional area of 7 cm^2.

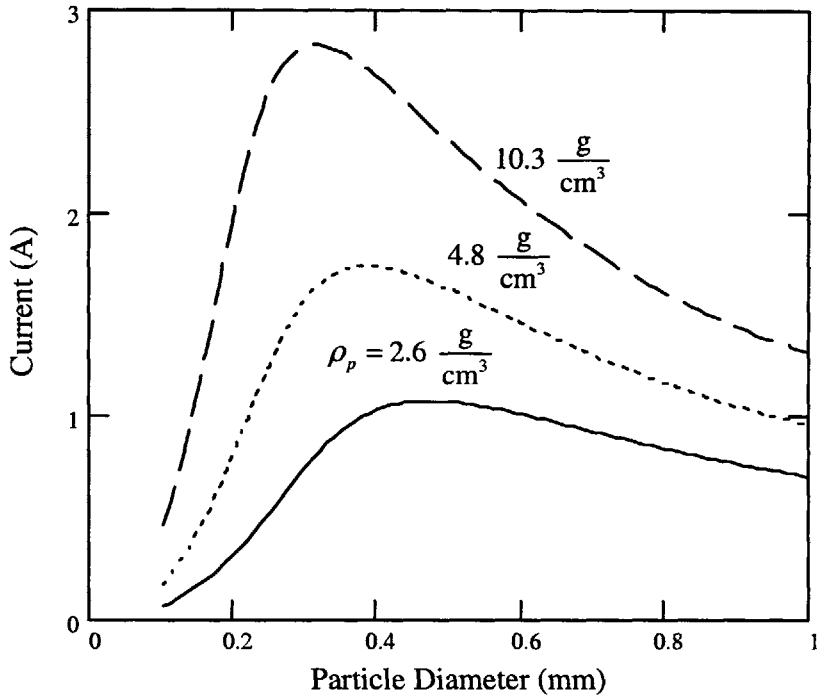

Figure 6: Effect of particle density on current output as a function of particle diameter. The bed and electrolyte parameters otherwise are those given in Table 5 and Table 10. The bed is 1 cm long, has a cross-sectional area of 7 cm^2, and a level of fluidization of 15%.

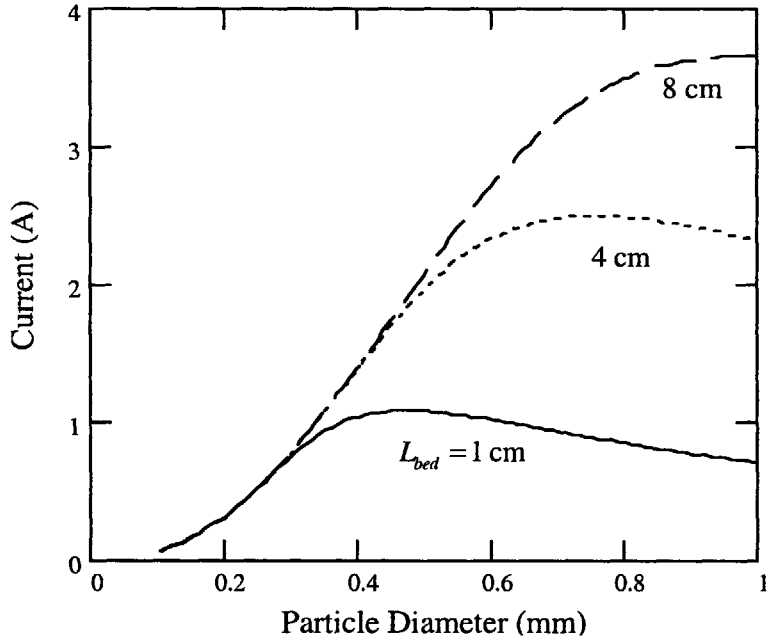

Figure 7: Effect of bed length on current output as a function of particle diameter. The bed and electrolyte parameters are those given in Table 5 and Table 10. The bed has a cross-sectional area of 7 cm^2 and a level of fluidization of 15%.

The trends in Figures 5 to 7 are expected. Performance improves as the fluidization, and thus velocity, increases. Performance also improves as the density of the particles increases, since the mass transfer coefficient and the velocity the bed can tolerate for a given level of fluidization both increase. The influence of length increases performance since there is more active surface area in the bed. The electrode, now with greater surface area due to length, opts for larger particles that will allow for a greater electrolyte velocity, even though they have less surface area.

Note that equation (30) represents an upper bound on actual performance. The practical optimum must also take into account voltage, which the model does not consider. Figure 5 suggests that the optimum particle size is slightly smaller than that used in reference [14] when higher levels of fluidization are used. When considering voltage, however, smaller particles can lead to higher resistances in the bed due to the increased contact resistance between the greater numbers of particles in a given volume. The authors of reference [13] recognized this trend in a set of experiments designed to also determine the optimal particle size. Keeping the current output of the electrode constant, they measured the overpotential for various particle diameters. Of the particles they tested, a diameter of 0.6 mm produced the smallest overpotential for the required current; the actual optimum according to their graph appears to be around about 0.8 mm. The larger overpotentials required by their data for smaller particles suggest that a sub-optimal result of a larger particle for a given set of conditions may be required to offset the ohmic resistance within the electrode. Note, however, that larger particles are not the only way to reduce contact resistance. Particles composed of a conductive metal, rather than glass, would be another way to decrease contact resistance and shift the optimum based on voltage closer to the true optimum given by the model.

7.0 The Upper Limit of Fluidized Bed Electrode Performance

We would like to establish an upper limit for the performance of the fluidized bed electrode that we can then compare to other electrode designs. In order to do this, however, reasonable estimates for the optimum level of fluidization and the voltage at which the fluidized bed electrode will run need to be decided upon. In this section, these values are determined, and the model is then used to predict optimal performance.

7.1 Level of Fluidization and Operating Voltage

Lacking other resources, the optimum value of fluidization has to be determined from the data of past research. As mentioned in Section 6.0, the higher the level of fluidization, the greater the ohmic resistance of the bed, and the higher the possibility for bed deactivation.

Both Berent et al. [13] and Matsuno et al. [7] conducted measurements of voltage drop throughout the bed. The anode tested in reference [13] could go up to 10% fluidization without any deactivation. The anode, however, was more resistive than the cathodes tested in reference [13]. The cathode experiments showed some sign of bed polarization at a fluidization of 16.6% but no deactivation. The fluidized bed of reference [7] showed no voltage drop in the bed or deactivation for up to about 10% fluidization (even though

as explained in section 5.5, the fluidization in this bed was probably caused by bubbling, not by electrolyte flow and thus the results may not directly relate). The data in reference [14] go to a maximum of 25% fluidization. At this level of fluidization, however, the voltage of the electrode had to be driven to almost 1 Volt in order to reach the limiting current. Again, the particles used in reference [14] were glass beads with a silver coating as the catalyst. If a highly conductive material such as silver had been used for the beads themselves as in reference [7], then the bed might have been able to tolerate these higher levels of fluidization. Lacking more information, a fluidization of 25% will be used as the upper limit in the following sections, realizing that in actual practice, the level of fluidization might have to be less than 25%.

In optimizing the output of the electrode, it is necessary that the pump power be included in the model. In order to convert the current output obtained by equation (30) into a power measurement, an estimate for the operating voltage of the fuel cell needs to be determined. For the hydrogen-oxygen reaction, the reversible potential for an alkaline electrolyte fuel cell is 1.23 volts. Due to the losses discussed in Section 2.1, the voltage is never this high in the cell. Often, the value of the voltage that maximizes power in a fuel cell is between 0.5 and 1 V; the voltage operating points quoted in the fuel cell data of reference [3] are mostly 0.6 V or 0.7 V for ambient PEM fuel cells. In reference [18], maximum power is obtained around 0.7 V. To determine the actual value for a fuel cell employing fluidized bed electrodes would be a complicated process, but the performance of a fuel cell employing fluidized bed electrodes is expected to be no better than a typical cell if not worse (see Section 10). Thus 0.8 volts is chosen as an upper limit value for the fluidized bed electrodes.

In summary, the properties of the fluidized bed electrode that are used to optimize electrode performance in the following sections are given in Table 11. Note that the particles are now being modeled as solid silver. The properties of the electrolyte given in Table 5 are also used in the following sections.

Table 11: Fluidized Bed Parameters

Voidage, ε_{mf}	Cross sectional Area (cm^2)	Particle Density, ρ_p (g/cm^3)	Level of Fluidization	Voltage (V)
0.42	1	10.3	25 %	0.8

7.2 Equations to Model the Power Output of a Fluidized Bed Electrode

Assuming the pump has an efficiency of 100%, then the power required by the pump is simply

$$P_{pump} = \Delta p \cdot \dot{V} \tag{31}$$

where Δp is the pressure drop across the bed. The generated power, produced by the reaction of the fuel cell is

$$P_{generated} = E \cdot i_{\lim} \tag{32}$$

where i_{lim} is given by equation (30) and E is the voltage of the cell, or 0.8 V. The one modification to equation (30) is that instead of solving for the value of k_m using the lower bound of equation (9), which is equation (13), the upper bound in equation (9) is used instead. The difference is small, but done for completeness, since the ultimate goal is to find the upper limit in performance of a fluidized bed electrode. The net power produced by the fuel cell is then

$$P_{net} = P_{generated} - P_{pump} \tag{33}$$

One of the great advantages of fluidized beds is that the pump power is low. For the relatively short beds considered in this analysis, the pump power is almost negligible. Regardless, we include it in some of the graphs for completeness. The pump power is again shown in equation (31), where the pressure drop in the fluidized bed electrode is given by [16]

$$\Delta p_{fbe} = L_{bed}(1-\varepsilon)(\rho_p - \rho_f)g \tag{34}$$

where L_{bed} is length of the bed.

7.3 The Upper Limit of Fluidized Bed Performance: Results of the Models

The result of plotting equation (32) as a function of diameter for various lengths is shown in Figure 8. The power output in all of the following graphs is given per square centimeter of the cross-sectional area of the electrode in the direction perpendicular to flow. The values of the various parameters are given in Tables 5 and 11. In Figure 9 the power as a function of diameter is plotted for two electrode lengths with and without the pump power included, equations (33) and (32) respectively. In Figure 9, "net" designates that the pump power is included.

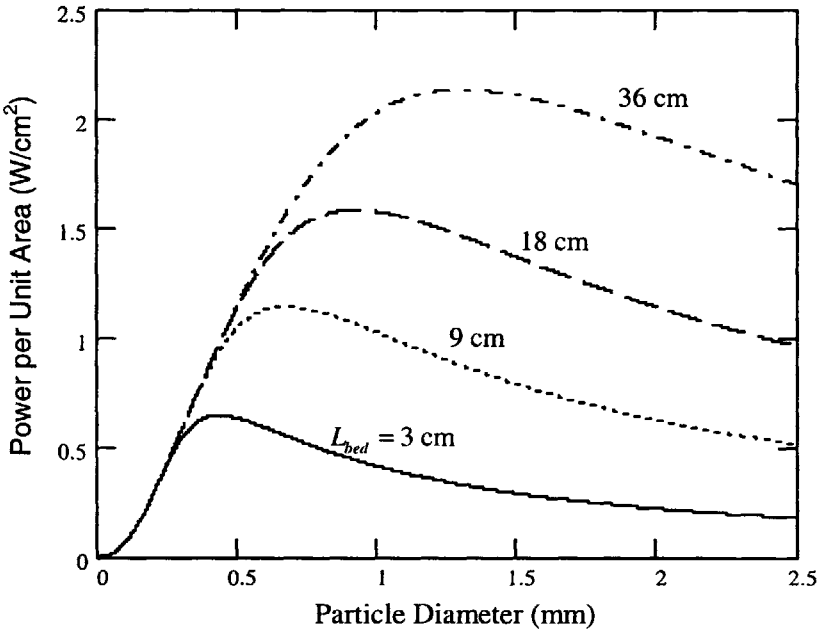

Figure 8: Variation of power output of a fluidized bed electrode with particle diameter for various electrode lengths. The values of the various parameters are given in Tables 5 and 11.

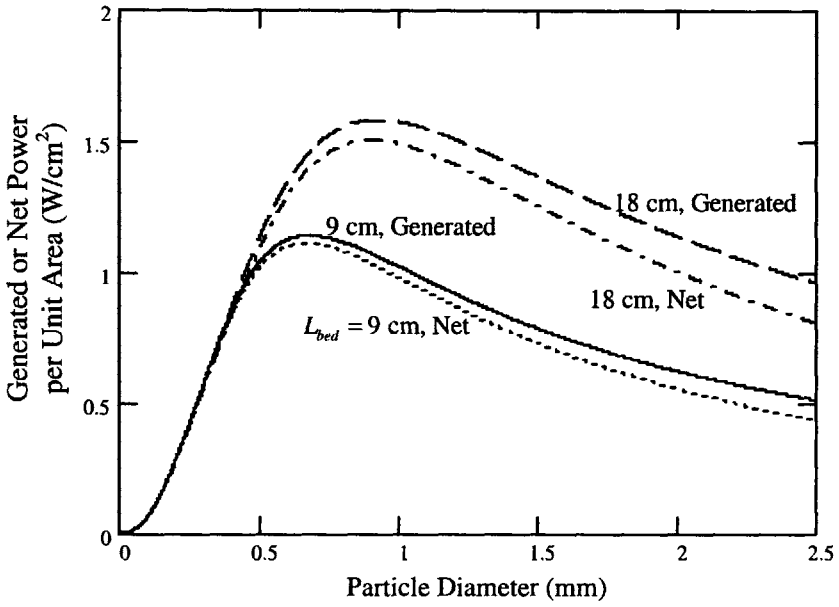

Figure 9: Variation of power output of a fluidized bed electrode with diameter for electrode lengths of 9 and 18 cm with and without the pump power considered. In the figure, "net" designates that the pump power is considered. The values of the various parameters are given in Tables 5 and 11.

For an electrode 9 cm long, Figure 10 presents the ratio of available power to the total power produced, which is the efficiency of the electrode, and the fraction of power that is consumed by the pump. Figure 10 also depicts the fraction of O_2 consumed in the bed for a given diameter at electrode lengths of 9 cm and 18 cm. Figure 11 presents the superficial velocity required to reach 25% fluidization for the range of particle diameters presented in the other graphs. Figure 12 shows the variation of power output of a fluidized bed electrode with particle diameter for an electrode length of 9 cm and various percentages of the value of the velocity given by equation (29). The value of the expected velocity in Figure 12 is varied by plus or minus 25%, which is the maximum of the error measured in Section 6.2. The pump power is not considered in Figure 12.

Figure 13 and Figure 14 show the variation of power output of a fluidized bed electrode with particle diameter for an electrode length of 9 cm and 1 cm respectively. Added to Figures 13 and 14 is the maximum power output that would be achieved if the electrolyte was always saturated with oxygen (for example, by bubbling). This limit is referred to as the transport limitation since the performance is ultimately limited by the rate of mass transport to the particles in the bed, which depends on the area and the mass transfer coefficient. The transport limitation is determined by plotting equation (19) for the fluidized bed. Also plotted in Figures 13 and 14 is the maximum power if the transport rate was infinite but the only source of oxygen was that transported into the bed by the electrolyte (supply limitation). The supply limitation is calculated by letting the exponential term in equation (17) go to zero. The pump power is not considered in Figures 13 and 14.

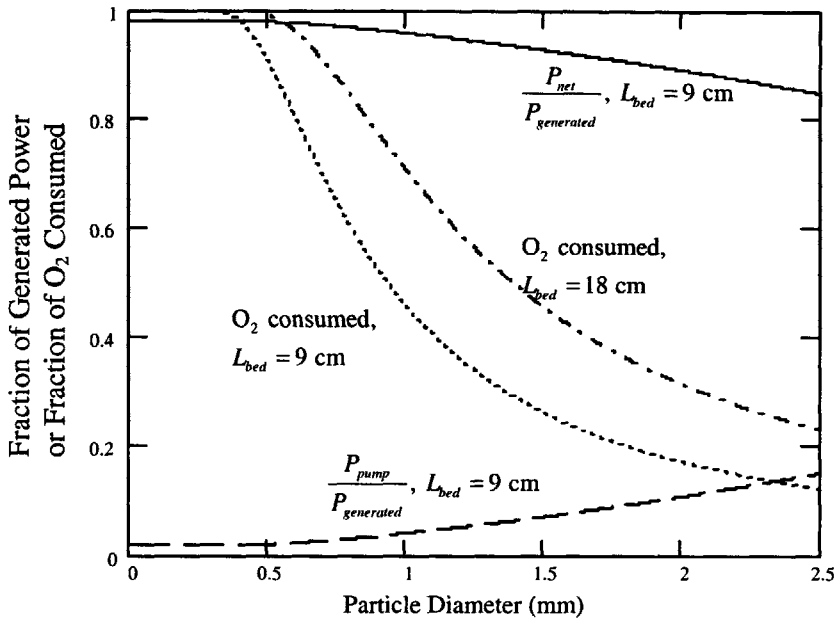

Figure 10: The efficiency of the electrode, defined as the net power divided by the total power produced, and the fraction of the generated power required to operate the pump for an electrode length of 9 cm. Fraction of O_2 consumed in the bed for a given diameter at an electrode length of 9 cm and 18 cm is also given.

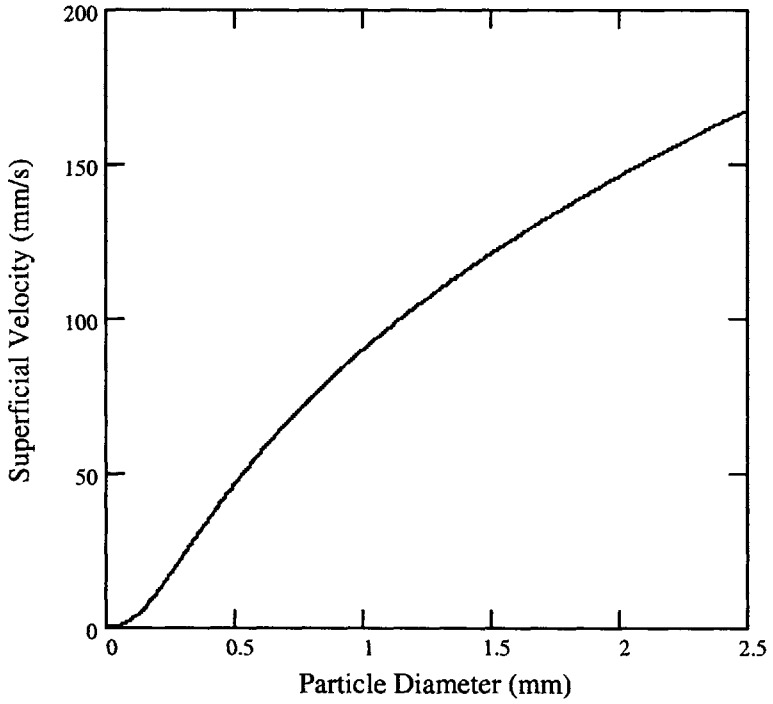

Figure 11: Velocity for a given diameter in the fluidized bed with 25 % fluidization. Relevant parameters are given in Tables 5 and 11.

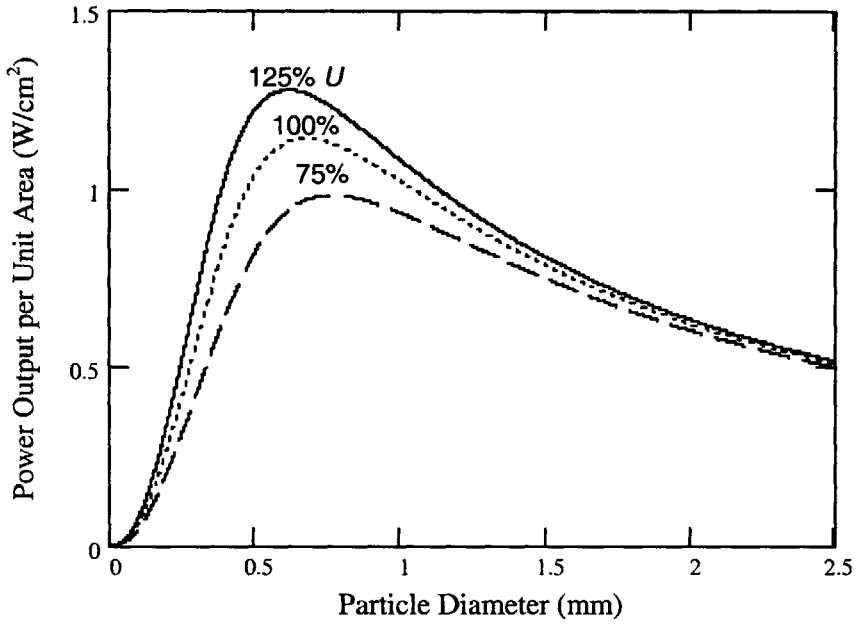

Figure 12: Variation of power output of a fluidized bed electrode with particle diameter for an electrode length of 9 cm and various percentages of the value of the velocity given by equation (29). Pump work is not considered. The values of the various parameters are given in Tables 5 and 11.

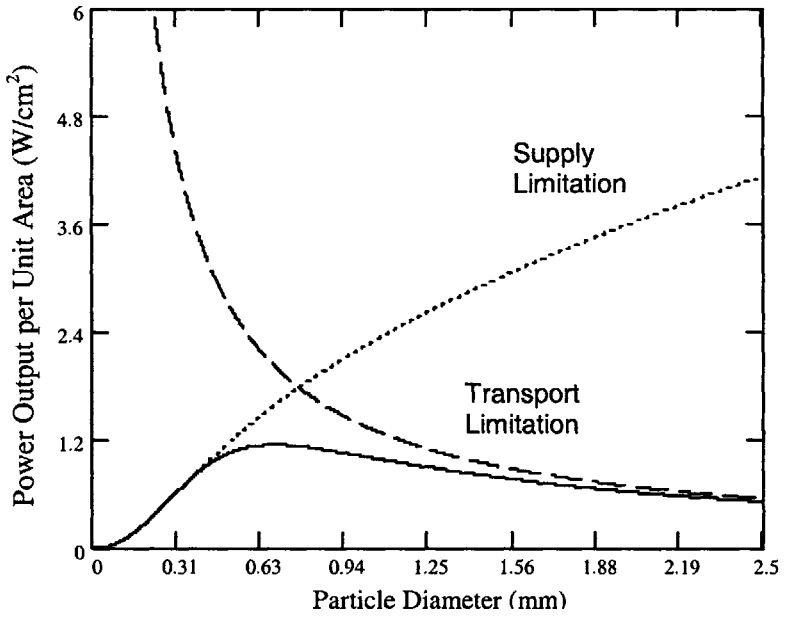

Figure 13: Variation of power output of a fluidized bed electrode with particle diameter for an electrode length of 9 cm. Also plotted are the maximum power if the electrolyte was always saturated (transport limitation) and the maximum power if the area was infinite but the only source of oxygen was that transported into the bed by the electrolyte (supply limitation). Pump power is not included.

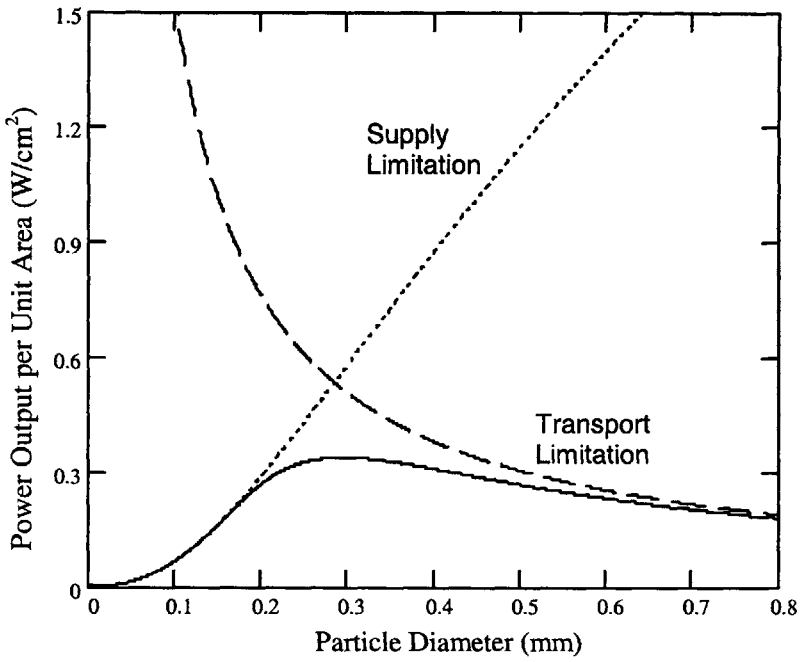

Figure 14: Variation of power output of a fluidized bed electrode with particle diameter for an electrode length of 1 cm. Also plotted are the maximum power if the electrolyte was always saturated (transport limitation) and the maximum power if the area was infinite but the only source of oxygen was that transported into the bed by the electrolyte (supply limitation). Pump work is not included.

7.4 Discussion of the Results

Figure 9 depicts that only for very long electrodes and large particle diameters, does the pump power affect the results significantly. Figure 10 confirms this observation. At the optimum particle diameter for the 9 cm electrode, the pump power is only a few percent of the total power generated.

The overall trend in the results of Figure 8 is that as the electrode length increases, the optimum particle size increases as electrode area is traded for greater electrolyte velocities. The optimum occurs at the same percent of oxygen consumed (about 75%), regardless of electrode length, as can be determined from the data in Figure 10 for 9 cm and 18 cm long electrodes.

The velocity of the electrolyte that maximizes power for a 9 cm long electrode is around 60 mm/s, according to Figure 11. This velocity is large compared to the velocities used in past studies on fluidized beds.

Figures 13 and 14 clearly show that outside of the optimal diameter region, current is either limited by supply or by the product of the mass transfer coefficient and the surface area. Figure 13 shows that for an electrode length of 9 cm, any particle size greater than about 1 mm in diameter quickly becomes limited by the lack of surface area in the bed for that length of electrode. Any particle size less than 0.5 mm is limited not by surface

area, but by the amount of oxygen carried into the bed by the electrolyte. As the particle size decreases, the velocity has to decrease, so the supply of reactant into the bed decreases. Thus the optimum occurs when the mass transport and the reactant supply balance; that is, when $A_S k_m$ is roughly equal to $\dot{V}$.

Figures 13 and 14 also show the limits for a 3-phase bed. In an ideal 3-phase bed, the maximum due to the supply limitation is removed, and the electrolyte is always ideally saturated with oxygen. The maximum for a 3-phase bed would then occur along the transport limitation line at the smallest particle size that can tolerate the bubbling in the bed. Bubbles moving through the bed tend to entrain particles, especially as the particles become very small. Reference [13] initially tried to fluidize a bed with gas as well, but gave up due to the extreme difficulty in stabilizing a 3-phase bed. References [7] and [4] did use a 3-phase bed, but their results appear to be at liquid velocities below the minimum fluidization velocity, and their studies employed large particles. The optimum would thus occur when the improvement due to smaller particles is offset by the effect of entrainment and bed instability. Again, note also that the study in reference [13] found that the ohmic resistance in the bed seemed to increase for very small particle sizes. The ohmic resistance due to particle-to-particle contact thus may also affect the optimum.

The power density (W/cm^3) can be determined from Figure 14, for an electrode 1 cm in length. For the two-phase bed, the power density has a value of about 0.35 W/cm^3 at this length. If the bed was 3-phase and ideally saturated, and the particles could be as small as 0.1 mm without significant adverse affects, the power density would increase to 1.5 W/cm^3.

7.5 The Design of Fluidized Bed Electrodes

From the results of the last section, several clear trends are observed for how the electrode parameters affect performance of the fluidized bed electrode and what values result in a good design.

It can be concluded from the results of our analysis that particles of high density are best. From the data of previous investigators, it also seems clear that highly conductive particles are beneficial. According to the analysis in Section 5.3, porous particles should probably not be used, at least not Raney-type; the high surface area is not utilized and the porosity decreases the particle density.

The optimum particle diameter depends on several factors. For an ideal two-phase fluidized bed electrode, where fluidization stability and voltage drop in the bed are not a concern, the particle diameter varies with the bed length. The optimum occurs approximately when $A_S k_m$ is equal to $\dot{V}$. In actual practice however, if the bed is short and small particles are required, the particle size that produces the best performance may occur at a particle diameter that is suboptimal according to the model but necessary to ensure bed stability and minimize the voltage drop in the electrode. The model serves as an adequate first guess at optimum particle size.

For a three phase fluidized bed electrode, the optimum will tend toward smaller particle sizes since the reactant is bubbled into the bed and the high velocities required to deliver reactant are thus not as important. The advantage of a three-phase fluidized bed in practice is still unclear however. The results of reference [4] analyzed in Section 5.3 seem to indicate that the gas phase does not keep the electrolyte saturated as desired. If a lower electrolyte velocity is indeed required to deal with the stability issues noted in reference [13], then the third phase might be more harmful than beneficial. The entrainment issues and voltage drop due to smaller particles might both quickly outweigh any advantage of the three-phase bed. If however the bed is made long, so that large particles can be used, the stability issues may not be a concern. With a long bed however, the power density will quickly decrease; whether or not a lower power density is a problem will depend on the application.

For a two-phase fluidized bed electrode, the highest power density occurs in a bed that is as short as possible. The practical issue with a short bed is that in order to generate significant power, there has to be a large number of electrodes. Thus, the fluidized bed supporting structure has to be repeated and there must be space between electrodes for hardware used to re-saturate the electrolyte with oxygen. This extra space is volume not used for producing power, and thus reduces the power density of the fuel cell. The design of the distributors will also have a greater effect on a shorter bed since entrance effects will be more pronounced.

8.0 Packed Beds

An alternative to compromising between a higher electrolyte velocity and a larger surface area is to hold the particles in place and run the electrode as a fixed, or packed, bed. In a packed bed, deactivation of the particles due to disconnection from the bed is no longer a concern. Also, the orientation of the bed with respect to gravity is not an issue, so that this bed may be applicable in situations where a fluidized bed might be harder to implement successfully.

The limitation to performance in the case of a packed bed electrode is the pump power. As the velocity increases, the power required by the pump to force electrolyte through the bed becomes prohibitively large. Just as in Section 7, an equation for the net power output of the bed can be derived and then optimized to find the possible performance from packed bed electrodes.

8.1 Mass Transfer and Pressure Drop in Packed Beds

In a liquid-solid packed bed, the mass transfer coefficient can be obtained from the correlation [22]

$$Sh = 2 + (1.1)Sc^{1/3}Re^{0.6} \tag{35}$$

where the Reynolds number is defined as

$$Re = \frac{U_{sf} d_p \rho_f}{\mu_f} \tag{36}$$

where U_{sf} is the superficial velocity into the bed, and the Sherwood number is defined as

$$Sh = \frac{k_{m\_pb} d_p}{D_{O_2}} \tag{37}$$

Using equation (12) to find the Schmidt number and then combining equations (35) through (37), the expression for the mass transfer coefficient for a packed bed can be obtained:

$$k_{m\_pb} = \frac{D_{O_2}}{d_p}\left[2 + 1.1\left(\frac{\mu_f}{\rho_f D_{O_2}}\right)^{1/3}\left(\frac{U_{sf} d_p \rho_f}{\mu_f}\right)^{0.6}\right] \tag{38}$$

In the packed bed, the pressure drop is given by reference [23]

$$\Delta p_{pbe} = \left(\frac{17.3}{Re} + 0.336\right)\frac{\rho_f U_{sf}^{\ 2} L_{bed}}{d_p}(1-\varepsilon)\varepsilon^{-4.8} \tag{39}$$

8.2 Performance of the Packed Bed Electrode

The mass transfer coefficient in equation (38) can be combined with equation (17) to produce an expression for the limiting current within a packed bed:

$$i_{\text{lim}} = zF\dot{V}C_{sat}\left\{1 - \exp\left(-\frac{D_{O_2} A_s}{d_p \dot{V}}\left[2 + 1.1\left(\frac{\mu_f}{\rho_f D_{O_2}}\right)^{1/3}\left(\frac{U d_p \rho_f}{\mu_f}\right)^{0.6}\right]\right)\right\} \tag{40}$$

where A_s is equation (16) multiplied by the total volume of the bed, and the volumetric flow-rate, $\dot{V}$, is again just equal to the superficial velocity U_{sf} multiplied by the cross-sectional area of the bed.

Substituting equation (40) into equation (32), we obtain an expression for the power generated by the packed bed. Substituting equation (39) into equation (31), we obtain an expression for the pump power. Equation (33) again gives the net power output of the electrode.

For the voidage of the packed bed, a value of $\varepsilon = 0.42$ is chosen, which is the same value as that used for the fluidized bed electrodes in Section 7. For the expected range of voidage for a packed bed, $\varepsilon = 0.42$ is an upper value. A voidage of $\varepsilon = 0.44$ is obtained when a packed bed is fluidized and then allowed to settle; a voidage of $0.359 \le \varepsilon \le 0.375$

is obtained by vigorously shaking or vibrating a packed bed [23]. A higher value of the voidage results in a higher limiting current.

In modeling the packed bed electrodes, the electrolyte properties are again given in Table 5. The only bed characteristics specified before the optimization are given in Table 12.

Table 12: Packed Bed Parameters

Voidage, ε	Cross sectional Area (cm^2)	Voltage (V)
0.42	1	0.8

8.3 Results of the Model

The optimum performance of the packed bed electrode depends on the length of the bed, the particle diameter, and the electrolyte velocity. The optimum was found by using three-dimensional plots such as that in Figure 15 of the net power output of the electrode as a function of both particle diameter and electrolyte velocity for a given length. The length was varied until an optimum was reached. It turned out that after a length of 4-5 cm, the output did not increase significantly with a greater electrode length. As the length increases, the optimum particle diameter changes in order to compensate. It was also found that the optimum occurred at essentially a constant velocity of 115 mm/s, regardless of the electrode length and diameter. The net power output for the electrode as a function of length and diameter is given in Figure 16 for a velocity of 115 mm/s.

For a length of 5 cm, a diameter of 0.32 mm optimizes net power. Figure 17 shows the generated, pump, and net power for a packed bed 5 cm in length and a particle size of 0.32 mm at various velocities. The efficiency of the electrode, defined as the net power divided by the total power produced, and the fraction of the generated power required to operate the pump are shown in Figure 18. The percent of available oxygen consumed is also shown in Figure 18. Since the velocity at the optimum of net power is always about 115 mm/s, in Figure 19 the velocity is held constant at 115 mm/s and the power density as a function of diameter for several different electrode lengths is plotted. Figure 20 shows the efficiency, pump work fraction, and percent O_2 consumed for a 1 cm long electrode employing particles of 0.12 mm diameter.

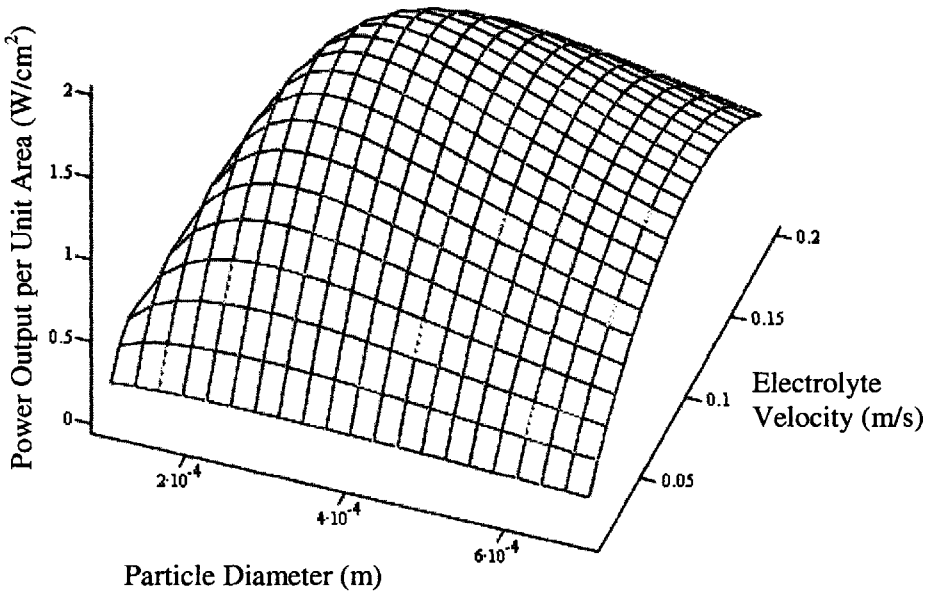

Figure 15: Net power output for a packed bed electrode as a function of particle diameter and electrolyte superficial velocity. Bed height is held constant at 5 cm.

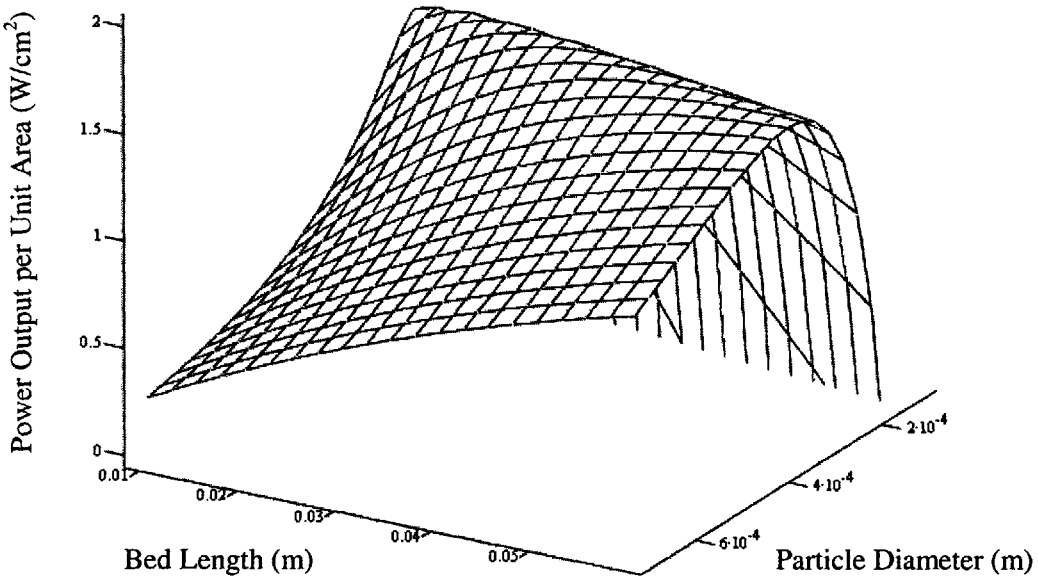

Figure 16: Net power output for a packed bed electrode as a function of bed length and particle diameter. Velocity is held constant at 115 mm/s.

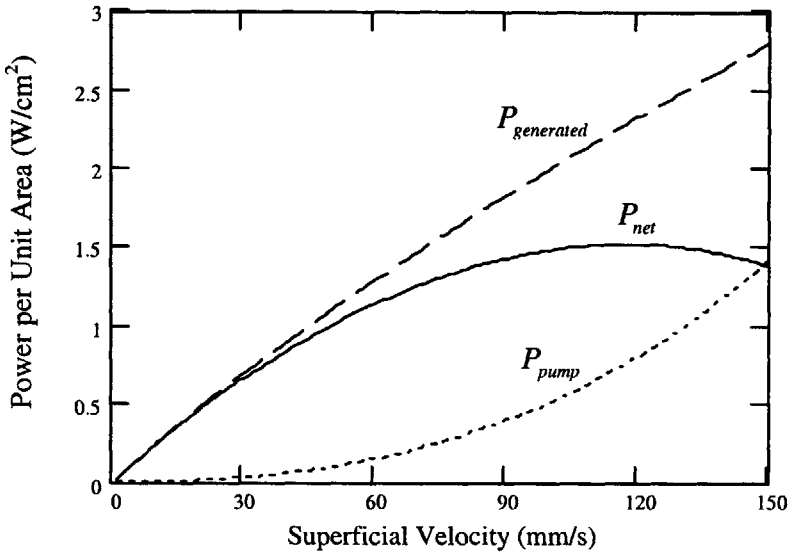

Figure 17: Generated, pump, and net power for a packed bed of 5 cm in length and 0.32 mm particle diameter.

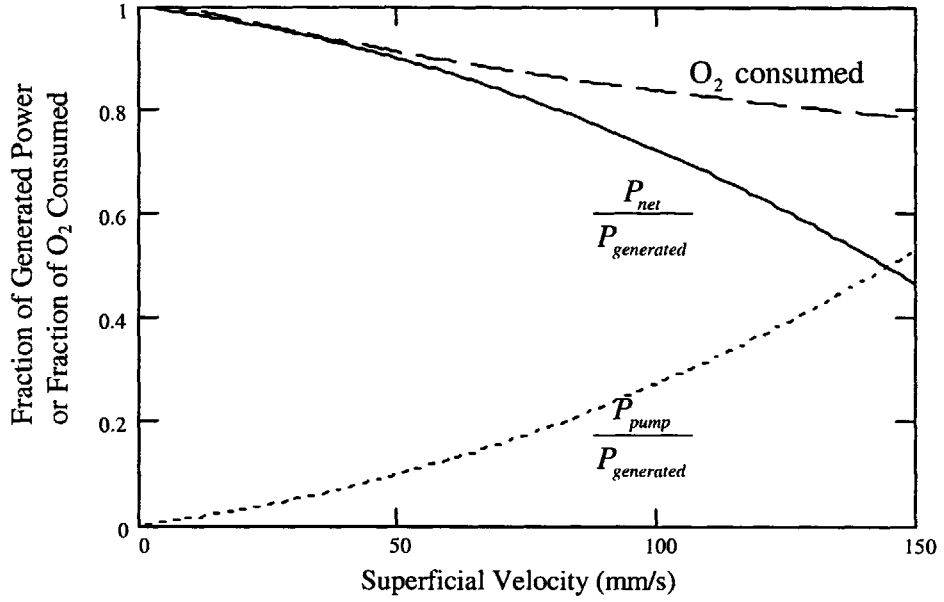

Figure 18: The efficiency of the electrode, defined as the net power divided by the total power produced, and the fraction of the generated power required to operate the pump for an electrode length of 5 cm with particles of 0.32 mm diameter. Fraction of O_2 consumed in the bed for various velocities is also given.

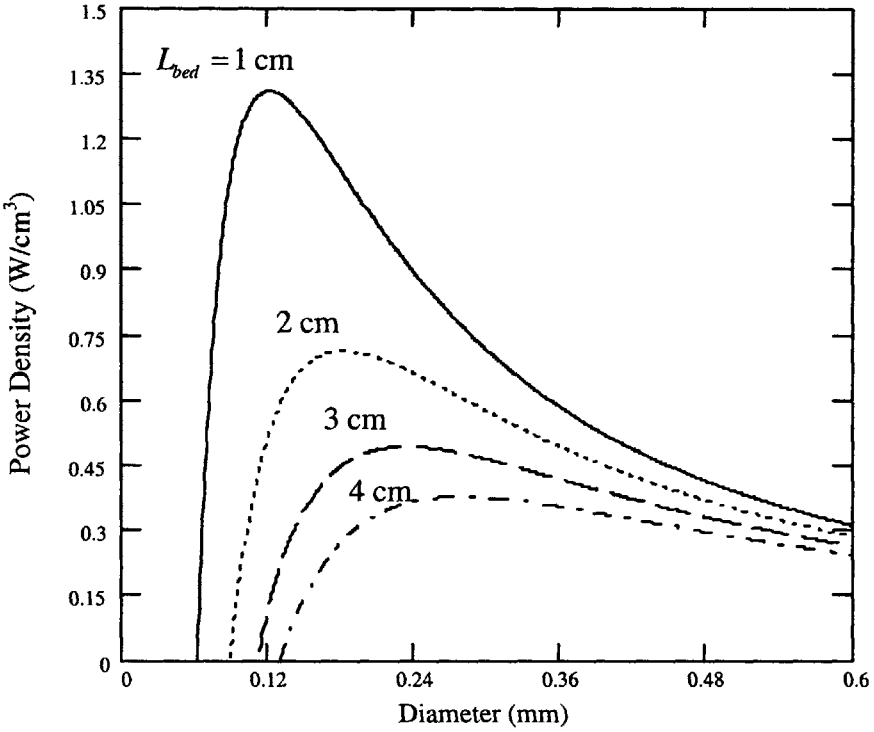

Figure 19: Net power density for a packed bed electrode for various particle diameters and electrode lengths. Velocity is held constant at 115 mm/s.

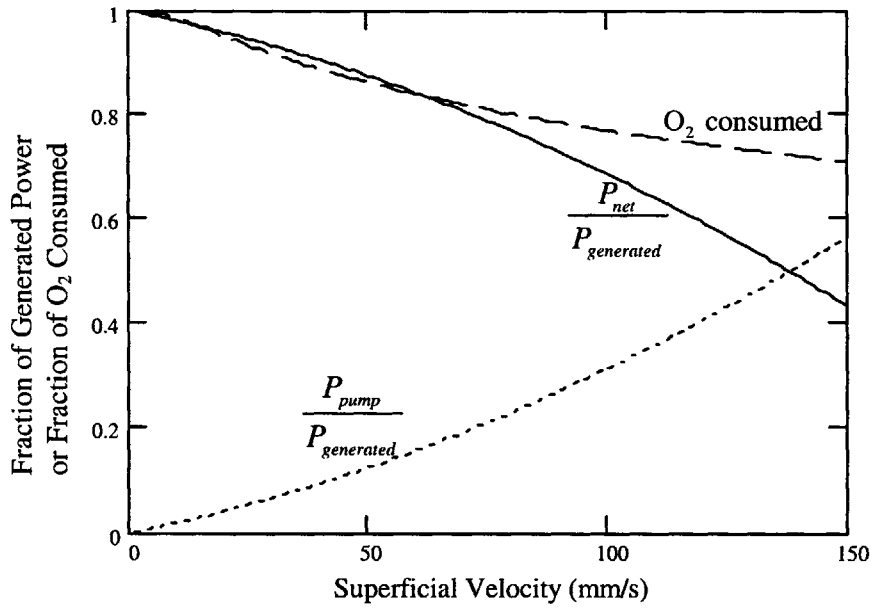

Figure 20: The efficiency of the electrode, defined as the net power divided by the total power produced, and the fraction of the generated power required to operate the pump for a packed bed electrode 1 cm in length with particles of 0.12 mm in diameter. Fraction of O_2 consumed in the bed for various velocities is also given.

8.4 Discussion of the Performance of Packed Bed Electrodes

The results of the optimization of the packed bed electrode in Figures 15 and 16 indicate that the power output doesn't increase indefinitely as the electrode is made longer, as in the case of a fluidized bed electrode, but reaches a maximum at about 3.5 to 4 cm in length. An electrode longer than 4 cm neither significantly improves nor decreases the net power output of the electrode. The particle diameter increases as the bed length increases in order to keep the pump power relatively low. This effect can be seen in equation (39), where the ratio of the bed length to particle diameter, L_{bed}/d_p, is essentially being held constant as the bed length increases. The Reynolds number in equation (39) also increases, which decreases the total pressure drop slightly, but this effect is minor and results in only a slight improvement in performance with bed length. As the particle diameter increases, the specific surface area of the particles drops, but because the length of the bed increases, the total surface area also remains about constant. The L_{bed}/d_p term appears in equation (40) as well if A_s is rewritten as the volume of the bed multiplied by equation (16).

Thus, for a particular particle diameter, the packed bed electrode has a finite length that optimizes net power output. As the length of the bed is increased past this optimum for a given particle diameter, more power is required to maintain the flowrate through the bed than is produced by the additional length of electrode.

The maximum of the packed bed electode occurs at a relatively high velocity, about 115 mm/s, compared to the fluidized bed data. At this velocity however, the efficiency of the electrode, defined as the net power divided by the total power produced by the electrode, is relatively poor at about 60%, as shown in Figures 18 and 20. As the velocity into the electrode is increased, the performance of the packed bed electrode improves due to both an increased supply of the reactant into the bed and an improved mass transfer coefficient. However, the increased velocity is achieved at the cost of a greater pressure drop and pump power.

As is clear from Figure 19, the maximum power density occurs when the electrode length is decreased to zero. For an electrode with a length of 1 cm, a power density of 1.3 W/cm^3 is achieved, but again, at an efficiency of about 60%. Interestingly, for the 1 cm and 5 cm packed bed electrodes, the maximum electrolyte velocities occur around 75 % O_2 consumed, which is close to the maximizing values seen in the fluidized bed electrodes.

9.0 Packed Screens

An alternative to the packed bed of particles is a packed bed of screens. Just as with the packed beds, the screen electrodes have a relatively large surface area per unit volume. The size of the wires of the screen, like the size of the particles in the packed bed, can be decreased to improve specific surface area. Just as with packed beds, the pressure drop will ultimately be responsible for limiting any further increase in velocity and thus performance. The performance of the screen electrode is evaluated in the following sections in order to provide another comparison to fluidized bed and packed bed

electrodes and to determine the advantages the screen electrode may have over the other designs, if any.

9.1 Screen Parameters

The screen considered in the following sections is a platinum screen produced by UNIQUE Wire Weaving Company. This same screen was used in reference [24] for testing flooded fuel cell performance. The mesh size, wire diameter, width of opening, and percent open area of this particular screen is given in reference [25] and reproduced in Table 13. In addition to those parameters listed in Table 13, the other parameter needed for the mass transfer and pressure drop correlations in the next section is the ratio of surface area to total area, which can be derived from simple geometric calculations using the notation in Figure 21.

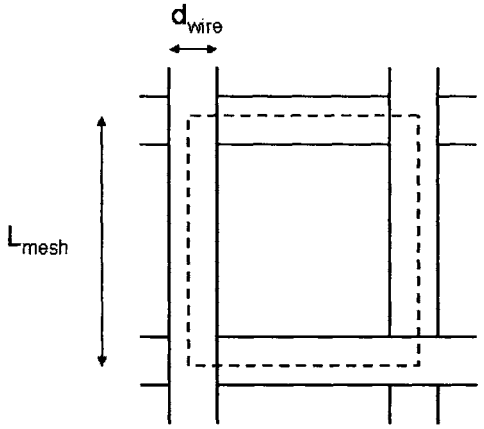

Figure 21: Schematic of a section of screen.

From the data given in reference [25], the width of the opening in Figure 21 is

$$L_{mesh} - d_{wire} = 0.127 \text{ mm} \tag{41}$$

The surface area of the portion of screen enclosed in the dashed box in Figure 21 is

$$A_{surface} = 2\pi d_{wire} L_{mesh} \tag{42}$$

The cross-sectional area of the dashed box is

$$A_c = \left(L_{mesh}\right)^2 \tag{43}$$

So then

$$\frac{A_{surface}}{A_c} = \frac{2\pi d_{wire}}{L_{mesh}} = 1.5942 \tag{44}$$

which is the ratio of the surface area of the screen to the cross-sectional area of the screen.

The ratio of the open area to total cross-sectional area (or percent open area) is defined in reference [26] as

$$\bar{f} = \frac{\left(L_{mesh} - d_{wire}\right)^2}{\left(L_{mesh}\right)^2} = 55.7\% \tag{45}$$

which is the same value given in reference [25].

The relevant parameters for the screen are summarized in Table 13.

Table 13: Properties of the Platinum Screen [25]

Mesh (wires/inch)	Wire Diameter (mm)	Width of Opening (mm)	Surface Area/ Total Area	% Open Area, $\bar{f}$
150 x 150	0.0432	0.127	1.6	55.5

9.2 Mass Transfer and Pressure Drop in Packed Screens

For a screen, the mass transfer coefficient is given by [24]

$$Sh = A_H Sc^{0.33} Re^{b_H} \tag{46}$$

where A_H and b_H are constants with values of 0.82 and 0.359 respectively. Substituting in for the Sherwood number:

$$k_{screen} \frac{d_{wire}}{D_{O_2}} = A_H Sc^{0.33} Re^{b_H} \tag{47}$$

where the Schmidt number is again defined by equation (12) and the characteristic length in the Reynolds number is based on the diameter of a wire of the screen:

$$Re = \frac{\rho_f U_{sf} d_{wire}}{\mu} \tag{48}$$

where U_{sf} is the superficial velocity into the screen.

Substituting k_{screen} into equation (17), an expression for the limiting current is obtained

$$i_{\lim} = zF\dot{V}C_{sat}\left\{1 - \exp\left[\frac{-D_{O_2} A_S A_H}{d_{wire}\dot{V}}\left(\frac{\mu_f}{\rho_f D_{O_2}}\right)^{0.33}\left(\frac{\rho_f U_{sf} d_{wire}}{\mu}\right)^{b_H}\right]\right\} \tag{49}$$

To determine the pressure drop, the velocity within the screen, U_{ws}, is used to define a Reynolds number

$$Re_{ws} = \frac{\rho_f U_{ws} d_{wire}}{\mu} \tag{50}$$

where the velocity in the screen can be determined by

$$U_{ws} = \frac{U_{sf}}{\bar{f}} \tag{51}$$

For values of $Re_{ws} < 50$, the pressure drop across one screen is then [26]

$$\Delta p_{screen} = \frac{\rho U_{sf}^{\ 2}}{2}\left(\frac{22}{Re_{ws}} + \zeta_{wire}\right) \tag{52}$$

where ζ_{wire} is a dimensionless pressure drop that depends on $\bar{f}$ and can be looked up in a table in reference [26]. For $\bar{f} = 55.7\%$, $\zeta_{wire} = 1.26$.

The thickness of the screen, which is the dimension of the screen in the flow direction, is not given. However, since the pressure drop does not depend on screen thickness, the only variable that will change with the thickness of the screen is the length at which the electrode is optimized; that is, if the screen is doubled in thickness, the optimum electrode length will double as well. A thickness of twice the wire diameter is chosen as a reasonable value of screen thickness. This thickness is expected to be about the thinnest that the screen can be made, and thus will provide an upper bound for the values of power density calculated by the model. The number of screens for a given length of bed is then

$$N_{screens} = \frac{L_{electrode}}{w_{screen}} \tag{53}$$

where w_{screen} is the width of the screen (= 2 d_{wire}).

The total pressure drop, as explained in reference [26] is just the pressure drop of one screen times the total number of screens, so

$$\Delta p_{total} = \Delta p_{screen} \cdot N_{screens} \tag{54}$$

The application of equations (54) and (49) to equations (31) to (33) give the pump, generated, and net power output for a packed screen electrode.

9.3 Results of the Performance of Packed Screen Electrodes

As was done with the packed bed electrode, the net power output of the screen electrode for a given electrode cross-section was first optimized. The net power output of the screen electrode depends on the length of the bed and the electrolyte velocity. The values in Table 5 are again used as the electrolyte properties. Figure 22 clearly shows that a single optimum exists for maximum net power produced by the electrode. It was found that an electrode 4.5 cm long produces the greatest power. An electrode longer than 4.5 cm uses more power pumping electrolyte through the additional length of screen than it

does gaining energy from the additional screen. The generated, pump, and net work output of the 4.5 cm long screen electrode are shown in Figure 23.

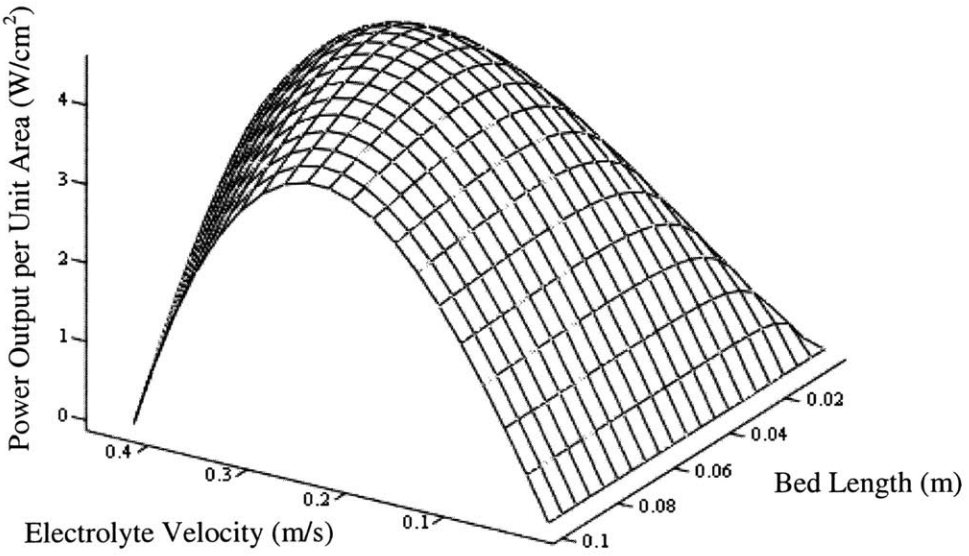

Figure 22: Net power output for a screen electrode as a function of bed length and electrolyte velocity.

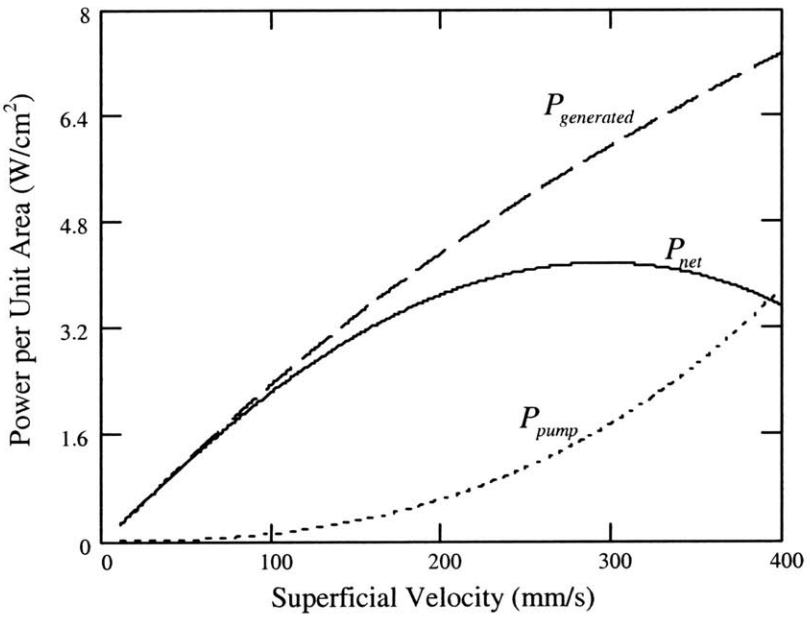

Figure 23: Generated, pump, and net power for a packed screen electrode 4.5 cm in length.

As was found with the packed bed electrodes, the optimum velocity in the packed screen electrode does not change significantly even as the electrode length changes. In the screen electrode, the optimum velocity is about 300 mm/s unless the electrode becomes

too long and the optimum is passed. Figure 24 is a plot of the generated, pump, and net power output of the electrode for various lengths with the electrolyte velocity fixed at 300 mm/s. Figure 25 is the same as Figure 24, except that the power density (power per unit volume), rather than power per unit area, is plotted versus length. That is, all values in Figure 24 have been divided by the respective lengths.

Figure 26 shows the efficiency, pump power fraction, and percent O_2 consumed for the 7 cm long packed screen electrode. Figure 27 shows the efficiency, pump power fraction, and percent O_2 consumed for a 1 cm long packed screen electrode.

Depicted in Figure 28 is a plot of net power per unit volume (as in Figure 25) for the packed screen electrode and for two packed bed electrodes for lengths of up to 3 cm.

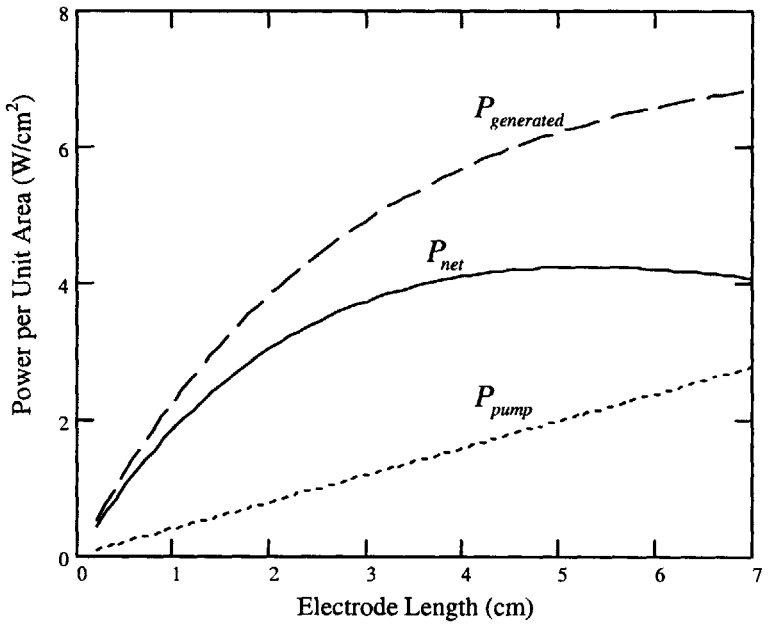

Figure 24: Plot of the generated, pump, and net power output of the electrode for various lengths. Electrolyte velocity is fixed at 300 mm/s.

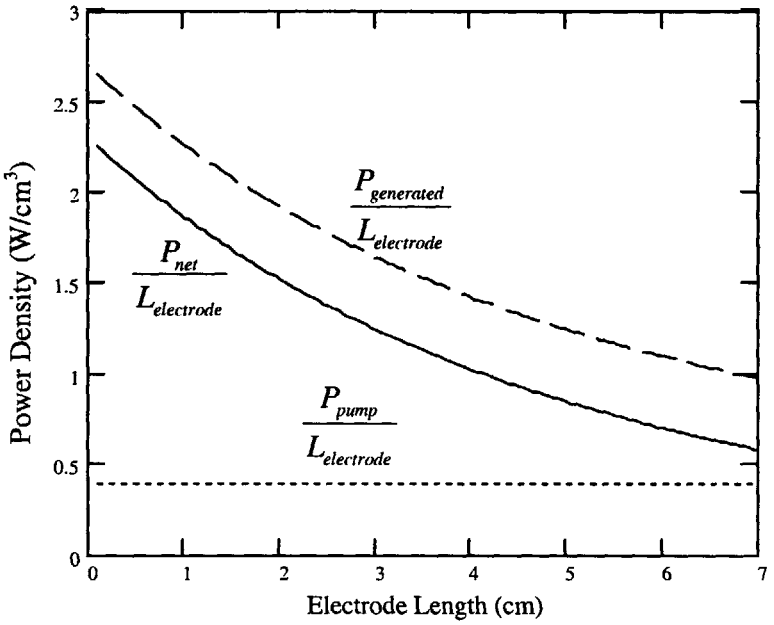

Figure 25: Plot of the generated, pump, and net power per unit volume of the electrode for various lengths. Electrolyte velocity is fixed at 300 mm/s.

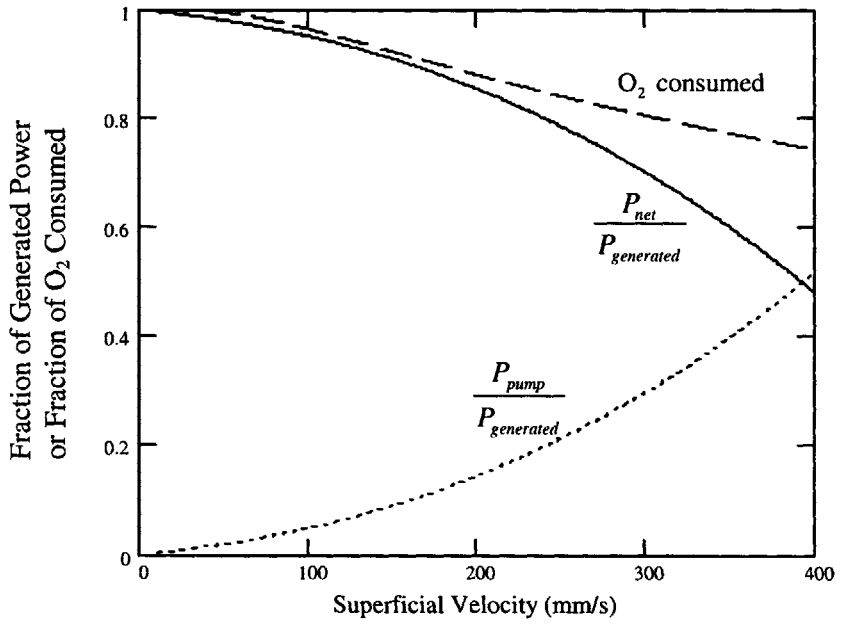

Figure 26: The efficiency of the electrode, defined as the net power divided by the total power produced, and the fraction of the generated power required to operate the pump for a packed screen electrode 4.5 cm in length at various velocities. Fraction of O_2 consumed in the electrode for various velocities is also given.

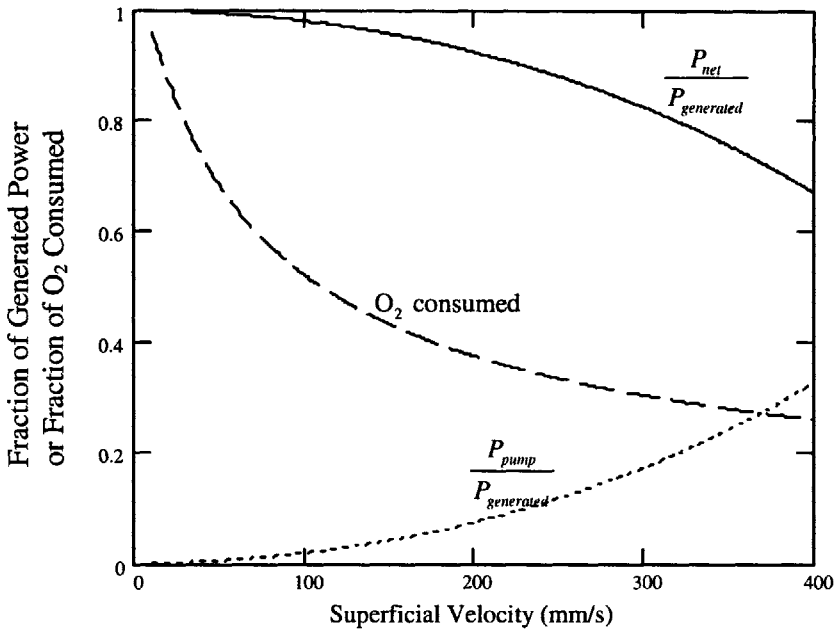

Figure 27: The efficiency of the electrode, defined as the net power divided by the total power produced, and the fraction of the generated power required to operate the pump for a packed screen electrode 1 cm in length at various velocities. Fraction of O_2 consumed in the electrode for various velocities is also given.

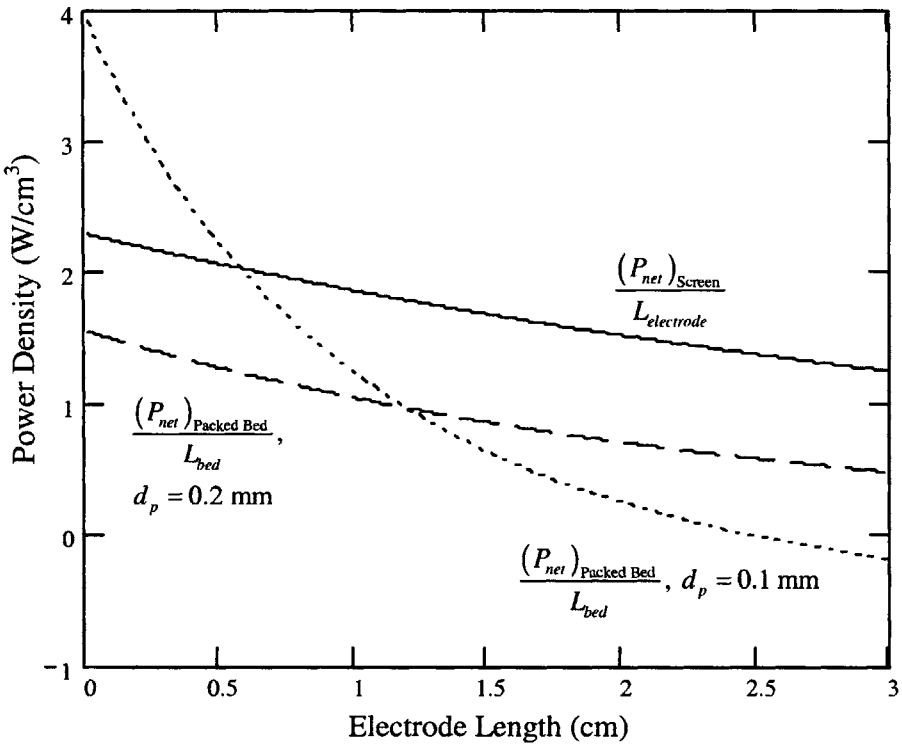

Figure 28: Power density of packed screen electrodes and packed bed electrodes of 0.1 mm and 0.2 mm particle diameter for various electrode lengths.

9.4 Discussion of the Performance of Packed Screen Electrodes

The maximum net power of the packed screen electrode occurs, according to Figure 23, at a velocity of about 300 mm/s, which is the fastest optimum velocity of the three electrode designs.

As depicted in Figure 24, the pump power increases linearly with electrode length, eventually reaching a peak at a length of about 5 cm. As with all the flooded designs, the generated power per unit length decreases as the electrolyte flows through the electrode and the concentration of oxygen in the bulk electrolyte decreases. Consequently, after about 5 or 6 cm in length, the additional power generated by a longer electrode is not enough to supply the additional power required by the pump, and the net power begins to decrease. The highest power density thus occurs for an electrode with a length of zero, as can be seen in Figure 25.

The packed screen electrode is capable of producing the greatest amount of power for an electrode greater than 0.5 cm in length of all the electrode designs (about 4 W/cm^2 versus less than 2 W/cm^2 for a packed bed electrode). When the electrode is reduced to less than 0.5 cm in length, however, the power density of the screen electrode becomes less than the power density of the fixed bed electrode, as shown in Figure 28. The screen electrode at very low lengths is unable to take advantage of the oxygen flowing through the electrode, and the percent of oxygen reacted drops to less than 25 %. The fixed bed in contrast is able to increase its area by decreasing the particle size to compensate for the short length. For a particle diameter of 0.1 mm, the packed bed has a higher surface area (314/cm) than the surface area per unit volume of the screen (185/cm). If a denser screen with smaller wires was used, a higher power density at electrode lengths less than 0.5 cm could probably be achieved. We have allowed for one more degree of freedom (the particle diameter) in the optimization of the packed bed than in the optimization of the screen electrode. Even with the extra constraint however, the screen performs better than the packed bed electrode for any length greater than 0.5 cm. This suggests that the screen electrode has an advantage compared to the packed bed electrode. Screen electrodes and other electrode types are further discussed in Section 11.

10.0 Voltage Loss and Complete Cell Performance

The model introduced so far has only depicted one aspect of the performance of a complete fuel cell: mass transport and the corresponding current limitation of the cathode. The true performance of the fuel cell depends on the voltage that the cell provides for a given current. The total voltage loss is a sum of the voltage losses in each electrode as well as in the electrolyte between them. The oxygen cathode has been the focus so far since in a typical hydrogen-oxygen fuel cell the cathode is the primary limitation. The line of thinking has been that if the limiting current of the cathode is poor, then there is no reason to complicate the matter further by trying to determine the voltage in the cathode as well, which is a much more difficult problem (especially in a fluidized bed cathode).

The output of the flooded electrodes discussed in the previous sections, in particular the packed bed and screen electrodes, is of the same order as the output of the PGD electrodes listed in Tables 1 and 2. Because the improvements suggested in Section 11 have the ability to improve performance further, it is important to consider the voltage drop in more detail, even if it is still from a simplified viewpoint.

In particular, of the three overpotentials discussed in Section 2.1, the voltage drop due to ohmic resistance for a fuel cell employing flooded electrodes may be more severe than in a typical PGD fuel cell. The past research in FBEs has made no mention of the ohmic overpotential, and the designs of the electrodes in these studies suggest that the ohmic loss was not considered. If ohmic losses had been considered, the electrodes probably would have been designed differently. In fact, the claim that the fluidized bed, or consequently any convection electrode, has some type of scale-up advantage would have been called into question, as it will be now.

As with the other parts of this thesis, we approach this issue by the development of simple models to predict upper bounds on performance. The relevant equations for modeling the ohmic overpotential are first introduced. Two simple models are then derived: one for the ohmic overpotential in a typical fuel cell, and the other as an upper limit for the ohmic loss in an alternative design. The last section describes how the new consideration of the ohmic loss in the following sections affects the previous results of mass transport for the various flooded electrode types.

10.1 The Voltage Drop due to Ion Mass Transport

The electrolyte between the two electrodes conducts an ionic current from one electrode to the other. The current that travels through the electrolyte must equal the current that the cell outputs to the load through the electrical connection in order to satisfy Kirchoff's current law at the electrode interface. According to Kirchoff's current law, the sum of the currents at the electrode interface must equal zero. In other words, all the charge that enters the electrode as electrons through the metal phase, must leave the electrode in the form of ions through the solution phase. There can be no buildup of charge in the steady state; what goes in must come out.

The current conducted by the electrolyte is a sum of the current carried by each ionic species within the electrolyte. The net current in a solution is then

$$i = \sum i_j \tag{55}$$

The current is produced by the mass flux of each species through the electrolyte. The flux of each species can be related to the current by the equation

$$i_j = -J_j z_j F A \tag{56}$$

where z is the charge on the ion, F is Faraday's constant (equal to 96485.3 C/mol), and A is the cross sectional area perpendicular to the flow of current.

The flux for each ionic species is given by [27]

$$J_i = -D_i \nabla C_i - \frac{z_j F}{RT} D_i C_i \nabla \phi + C_i \vartheta \tag{57}$$

where J is the molar flux per unit area (mol/m^2·s), D is the diffusion constant of the particular species, C is the concentration of the species, R is the molar gas constant, T is the temperature, and ϑ is the bulk velocity of the electrolyte. Note that ϑ is not necessarily the electrolyte velocity U in the previous sections.

Note that equation (57) is not strictly correct when applied to fuel cells. Equation (57) is for dilute electrolytes. Fuel cell electrolytes, however, are concentrated solutions. The driving force of mass flux in an electrolyte (of any dilution) is due to a gradient in electrochemical potential of the species within the solution. The approximation used in equation (57), which holds true only for infinitely dilute solutions, is that the electrochemical potential can be broken into a flux driven by the concentration gradient and a flux driven by the potential gradient. Due to the complexities that arise in modeling concentrated solutions using the electrochemical potential, researchers tend to use dilute solution theory instead, as was done in reference [18], in order to establish an approximation.

Thus the first term on the right-hand side of equation (57) accounts for the effect of diffusion due to the concentration gradient of the species in the electrolyte. The second term on the right-hand side accounts for the effect of migration, which is a driving force that acts on a charged species due to a potential gradient. The third term accounts for the mass flux of the species due to bulk convection of the electrolyte; that is, if the electrolyte is flowing, the species is going to be carried by that flow.

For a binary electrolyte, which is an electrolyte containing two types of ions, the total current conducted by the electrolyte can be determined by combining equations (55) and (56) to yield [27]

$$i = -J_+ z_+ FA - J_- z_- FA = FA\left(J_- - J_+\right) \tag{58}$$

Then applying equation (57),

$$i = FA\left[\left(-D_- \nabla C_- - \frac{z_- F}{RT} D_- C_- \nabla \phi + C_- \vartheta\right) - \left(-D_+ \nabla C_+ - \frac{z_+ F}{RT} D_+ C_+ \nabla \phi + C_+ \vartheta\right)\right] \tag{59}$$

Equation (59) can be simplified further by noting that the electrolyte has to be charge neutral at every point; there can be no net charge. This is an approximation, but a good one, as even negligible charge separation results in very large restoring forces [28].

Charge neutrality can be written mathematically as

$$\sum z_j C_j = 0 \tag{60}$$

For the KOH electrolyte, where $z_+ = 1$ and $z_- = -1$,

$$C_+ - C_- = 0 \tag{61}$$

$$C_+ = C_- = C \tag{62}$$

Hence the concentrations of potassium and hydroxyl ions everywhere must be equal. We can then write equation (59) as

$$i = FA\left[\left(-D_-\nabla C + \frac{F}{RT}D_-C\nabla\phi + C\vartheta\right) - \left(-D_+\nabla C - \frac{F}{RT}D_+C\nabla\phi + C\vartheta\right)\right] \tag{63}$$

Rewriting and grouping the terms

$$i = FA\left(D_+ - D_-\right)\nabla C + \frac{F^2A}{RT}\left(D_+ + D_-\right)C\nabla\phi \tag{64}$$

Note that the convection terms have canceled out due to the requirement of charge neutrality. This is an important result for fuel cells utilizing fluidized bed or convection electrodes. The velocity term in equation (57) seems to indicate that current can be carried by the bulk electrolyte. Thus one might assume that the ionic transport in convection electrodes can be improved, or at least tolerate greater separation between electrodes without a significant increase in the overpotential. Equation (64) reveals that no matter how much mixing occurs in a flooded fuel cell, the ionic transport is not improved; this is somewhat counterintuitive, but true due to the requirement of bulk charge neutrality.

In past studies of fluidized bed electrodes, this issue seems to have been completely ignored. The FBEs in past studies have been constructed as cylinders ranging from 2.5 to 5.1 cm in diameter. The typical spacing between PGD electrodes is less than 1 mm. Thus it seems that an ion generated by a reaction even just in the center of the 2.5 cm diameter electrode may have trouble making it to the edge of the cathode, let alone to the anode. The next two sections develop models to quantify the ion transport loss in various fuel cell configurations. These models indeed indicate that an electrode 2.5 cm in diameter is inappropriate.

10.2 Ionic Transport in Fuel Cells Employing PGD Electrodes

In a typical alkaline fuel cell, as depicted in Figure 1, the hydroxyl ion (OH^-) is the ion involved in the reaction. A hydroxyl ion is produced at the cathode and consumed at the anode. The other ion in solution is typically a potassium (or sodium) ion. Because the potassium ion is not consumed or produced at either electrode, the potassium ions have no net movement and thus carry no net current in the steady state:

$$J_+ = 0 = -D_+\nabla C_+ - \frac{z_+F}{RT} D_+ C_+ \nabla\phi + C_+\vartheta \tag{65}$$

Convection in the PGD electrode cell is considered negligible (as shown in the model in [18]), so eliminating the last term on the right-hand side, and then rearranging equation (65) results in an equation for the potential gradient as a function of the concentration gradient:

$$\frac{d\phi}{dx} = \frac{-RT}{FC_+}\frac{dC_+}{dx} \tag{66}$$

Where z_+ has been replaced by 1 and the equation has been modeled as one-dimensional.

The only flux that contributes to equation (55) is the movement of the negative ions, so

$$i = FA\left(-D_-\frac{dC}{dx} - \frac{z_-F}{RT} D_- C\frac{d\phi}{dx}\right) \tag{67}$$

where again the velocity term has been dropped, and charge neutrality, given by equation (62) has been applied.

Combining equations (66) and (67), an expression is obtained for the current only in terms of the concentration

$$i = FA\left(-D_-\frac{dC}{dx} - \frac{F}{RT} D_- C\frac{RT}{FC}\frac{dC}{dx}\right) \tag{68}$$

where z_- has been replaced by -1. Simplifying,

$$\frac{dC}{dx} = \frac{-i}{2D_-FA} \tag{69}$$

Thus the concentration profile for a given current is simply represented by a straight line.

The diffusion coefficients for both species depend on the concentration of the electrolyte at any given point according to the equations [18]

$$D_+ = \frac{D_e}{2(1-t_+)} \tag{70}$$

where t_+ is the transference number of the cation, equal to 0.298,

$$D_- = \frac{D_e}{2(1-t_-)} \tag{71}$$

where t_- is the transference number of the cation, equal to 0.702, and

$$D_e = 8.2263\times10^{-5} - 1.2271\times10^{-3}C_e^{0.5} + 4.2714\times10^{-2}C_e - 4.6387\times10^{-1}C_e^{1.5} + 1.66C_e^{2} \quad (72)$$

where C_e has the units of mol/cm^3, and D_e has units of cm^2/s. Equation (72) was created by the authors of reference [18] who performed a fourth order regression on the expected data points for diffusion coefficient data at 80 C. The points themselves at 80 C were extrapolated from diffusivity data at 25, 45, and 65 C.

Combining equations (69) and (71)

$$\frac{dC}{dx} = \frac{-i(1-t_-)}{D_e FA} \quad (73)$$

Equation (73) can be solved by rewriting it as

$$\frac{C(x+dx)-C(x)}{\Delta x} = \frac{-i(1-t_-)}{D_e(C(x))FA} \quad (74)$$

where D_e in equation (74) is evaluated at every point x using equation (72) starting with an appropriate initial condition. The initial condition is chosen so that the average concentration of electrolyte in the fuel cell is some pre-determined value.

Since equation (72) seems to hold reasonably well until an electrolyte concentration of about 0.5 M, and the value of D_e is essentially constant over the range of interest, equation (73) could alternatively be solved just by assuming D_e to be a constant and integrating. The result of solving equation (74) for an average concentration of 6 Molar at various current densities over a distance of 1 mm is given in Figure 29. The distance of 1 mm is chosen arbitrarily, but is expected to be an upper estimate of the actual distance in typical fuel cells. A distance of 1 mm is larger than the values used in the two confirmed models in reference [18], 0.05 mm and 0.5 mm respectively. Note the 0.5 mm value is assumed as a reasonable estimate by the authors in reference [18] due to a lack of other data.

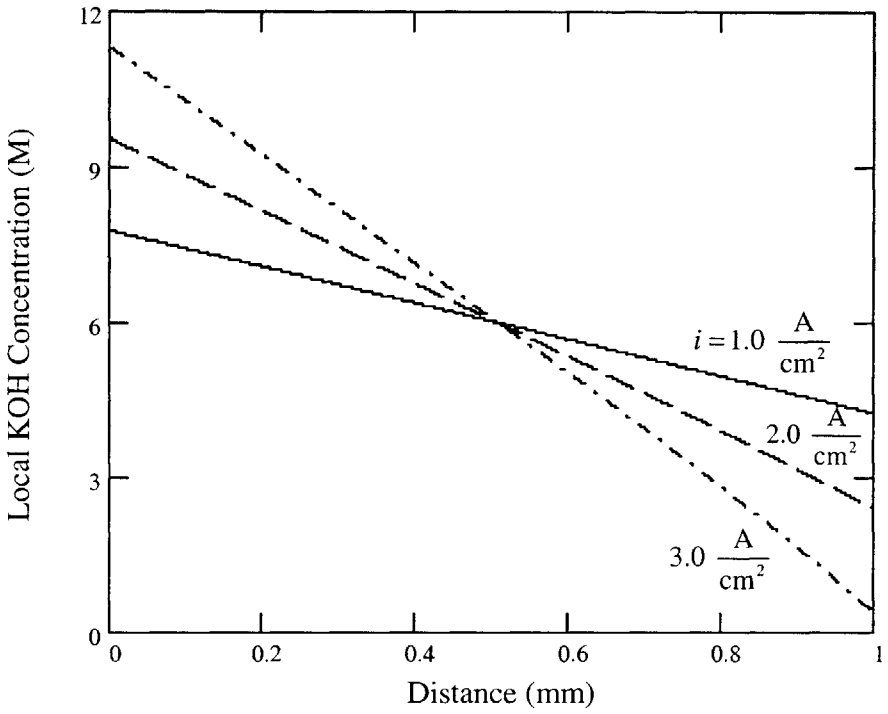

Figure 29: The variation in the concentration profile across a 1 mm distance at an electrolyte concentration of 6 Molar for various current densities.

Following the method of equation (74), equation (66) can be rewritten as

$$\phi(x+dx)-\phi(x)=\frac{-RT}{F}\left[\frac{C(x+dx)-C(x)}{C(x)}\right] \tag{75}$$

Equation (75) can be solved in the same manner as equation (74) using an initial condition for the potential of simply 0 V.

The results of equation (75) for the same conditions as in Figure 29 are shown in Figure 30. Alternatively, a current density of 1 A/cm^2 can be set, and then the concentration and potential variation for various values of the average electrolyte concentration can be plotted, as has been done in Figure 31 and Figure 32.

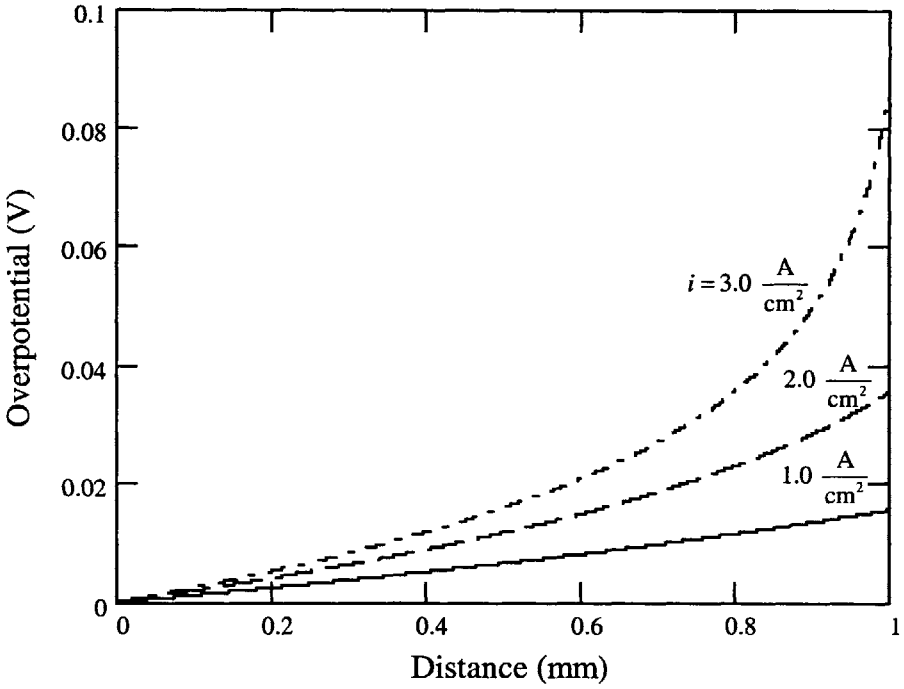

Figure 30: The variation in the potential across a 1 mm distance at an electrolyte concentration of 6 Molar for various current densities.

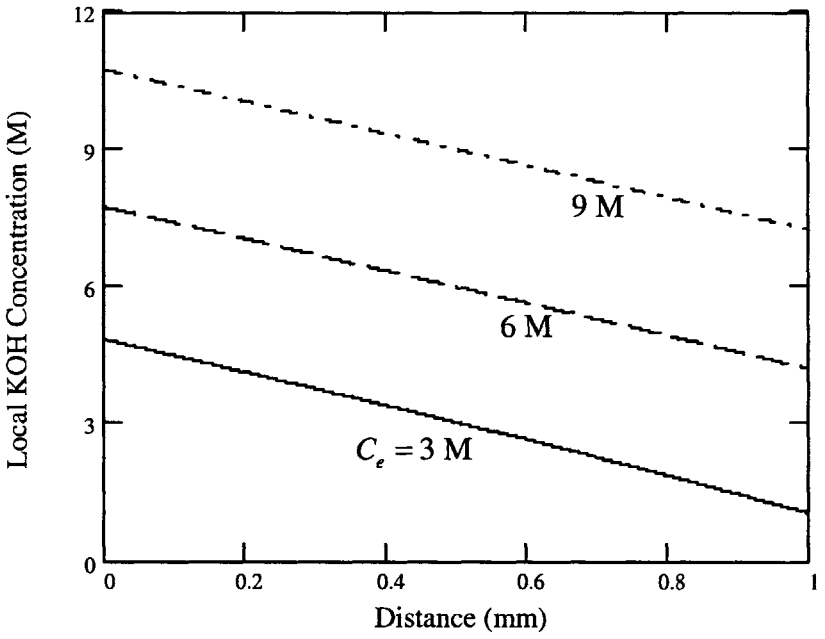

Figure 31: The variation in the concentration profile across a 1 mm distance for various electrolyte concentrations at a constant current density of 1 A/cm^2.

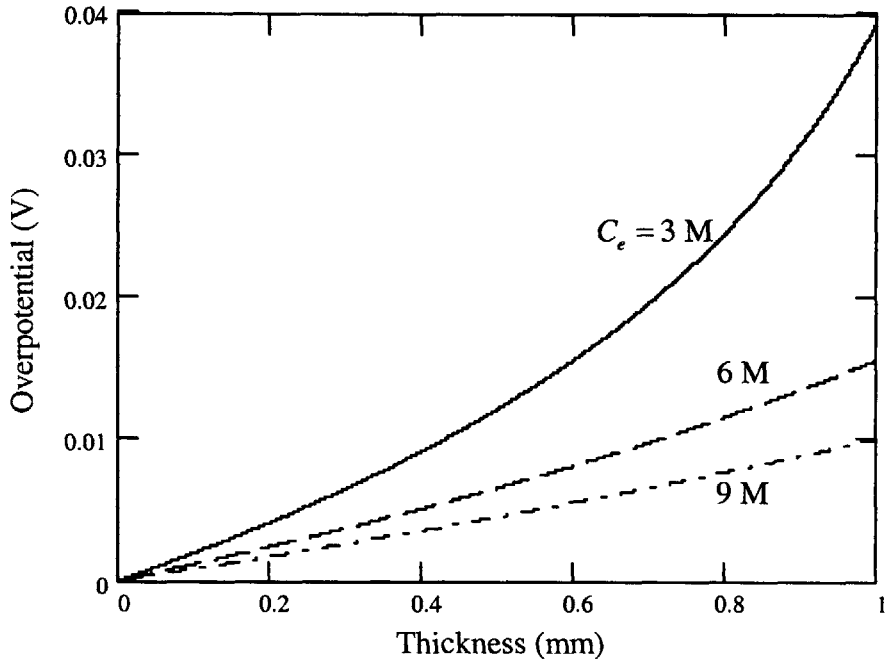

Figure 32: The variation in the potential across a distance of 1 mm for various electrolyte concentrations at a fixed current density of 1 A/cm^2.

The results of Figures 29 to 32 lead to several observations.

Observation 1: The influence of the various transport mechanisms becomes apparent from the concentration and potential profiles.
Figures 29 through 32 are plots for the concentration gradients and potential gradients in the electrolyte between the electrodes. Thus, Figures 30 and 32 clearly show that the potential of the cathode, which would be at the far left side of the graphs, is more negative than the anode, which is at the far right. The OH^- ions produced at the cathode are attracted to the more positive anode and thus migrate to the right. The higher concentration of the OH^- ions at the cathode, according to Figures 29 and 31, also causes the OH^- ions to move to the right by diffusion. Thus both migration and diffusion tend to move the OH^- ions to the right in each graph.

Migration due to the potential gradient causes the K^+ ions to move to the left, toward the more negative cathode; diffusion however causes the potassium ions to move to the right down the concentration gradient with the OH^- ions. The diffusion and migration of the K^+ ions cancel each other out, and the ions remain in place.

Thus the potential gradient is created primarily to maintain the charge neutrality of the solution, by counteracting the diffusion of the K^+ ions and keeping their concentration profile the same as the OH^- ion concentration profile. The added side effect of the potential gradient is an added boost to the current for a given concentration profile due to the beneficial migration of the OH^- ions.

Observation 2: The ohmic drop is relatively small.
Unless the electrode is run at high currents or with a low concentration of electrolyte, the drop in the potential across the 1 mm gap is very small. A similar result is seen in the data of reference [18] where at an operating voltage of 0.7 Volts and a total current of 2.2 Amps, the ohmic drop within the separator layer is only 7.6 mV, which is only 1.74% of the total cell polarization. The low ohmic drop calculated here can be a point of some confusion. In some literature, the slope of the voltage-current curve away from the initial activation overpotential and before the final concentration overpotential is linear. In [18], this region was calculated to have a slope of 0.081 ohms·cm^2. The drop in the voltage in the linear region is often labeled the "ohmic overpotential." As is clear from the discrepancy between the slope in this region in the data of reference [18] and the actual potential drop of only 7.6 mV in reference [18], the ohmic overpotential in this linear region is actually influenced by not only the ohmic resistance but also the kinetics and mass transport.

The voltage drop due to the ionic current is thus small even at the distances used in Figures 29 through 32 for most cases. In actuality, the thickness of the electrolyte layer would only be a fraction of the 1 mm used to plot the figures, and thus the overpotentials would be even smaller.

Observation 3: The ionic current can become limited by mass transport.
Note in Figure 29 that at a current of 3 A/cm^2, the concentration of the electrolyte at the anode is beginning to approach zero. As the potential is increased further, the concentration gradient eventually will reach a point where it cannot become any steeper. If the potential is increased beyond this point, the migration term would increase. However, since the concentration gradient cannot become steeper to keep the positive ions in place, the positive ions will begin to migrate to the cathode; since they cannot react at the cathode, they will simply accumulate. Ultimately, the added potential simply goes into separating the positive and negative ions from each other. Knowing that the forces due to even minor charge separation are large (hence the condition of charge neutrality), the current will not increase. Thus, once the concentration gradient reaches a maximum, the fuel cell will reach a mass transport limitation due to ion transport.

An ion transport limitation is not seen in typical fuel cells because of the thinness of the electrolyte layer and the high concentrations of electrolyte. However, the ion transport limitation would be prohibitively large for the fluidized bed electrodes used in previous work, especially at electrolyte concentrations of only 1 Molar, due to the large distance between electrodes. The ion transport limitation was not reached in these prior designs simply because the currents produced were so low.

The ion transport may be even worse in a fluidized bed electrode or any other type of electrode that relies on convective transport. In a PGD electrode, there is a substantial concentration gradient between the electrodes; this can be seen in the models developed in reference [18]. In a flooded electrode, however, that concentration gradient may be reduced due to mixing. The convection may not help carry current as shown in equation

(64), but it can certainly redistribute the charges. A reduced concentration gradient will only result in the ionic transport limitation being reached for an even lower current.

10.3 Ion Transport in Well-Mixed Cells

The electrolyte serves two purposes: to conduct a current between the two electrodes, and to transport the OH^- ions produced at the cathode to the anode. In the PGD electrode, both of these tasks are accomplished by the same mechanism; the OH^- ions conduct the current while diffusing and migrating from one electrode to the other.

The mass transport objective and current objective, however, can be decoupled. Consider the system in Figure 33. Assume that the electrolyte in both electrodes is strongly mixed, so that the concentration throughout the entire system is essentially the same. In this case, the diffusion terms in equation (64) are zero, since the concentration gradient is zero. Thus the only way that current can be carried from one electrode to the other is by migration. Since there is no concentration gradient to keep the K^+ ions in place, the K^+ ions slowly migrate from the anode to the cathode. The issue of K^+ ions accumulating at the cathode is solved in the system in Figure 33 by employing an ion return loop.

The ion return loop in Figure 33 takes electrolyte containing equal amounts of both K^+ ions and OH^- ions and transports them by bulk convection to the anode. The flow through the loop does not conduct current, since the species move together in equal amounts, but it does carry mass. It returns the K^+ ions to the anode, so that they can proceed to migrate back to the cathode, and it carries OH^- ions from the cathode to the anode to be consumed. Thus both ions can carry current by migration, and the K^+ ions will not accumulate at the cathode. The OH^- ions get to the anode by both migration and convection (and diffusion as well if there are concentration gradients present).

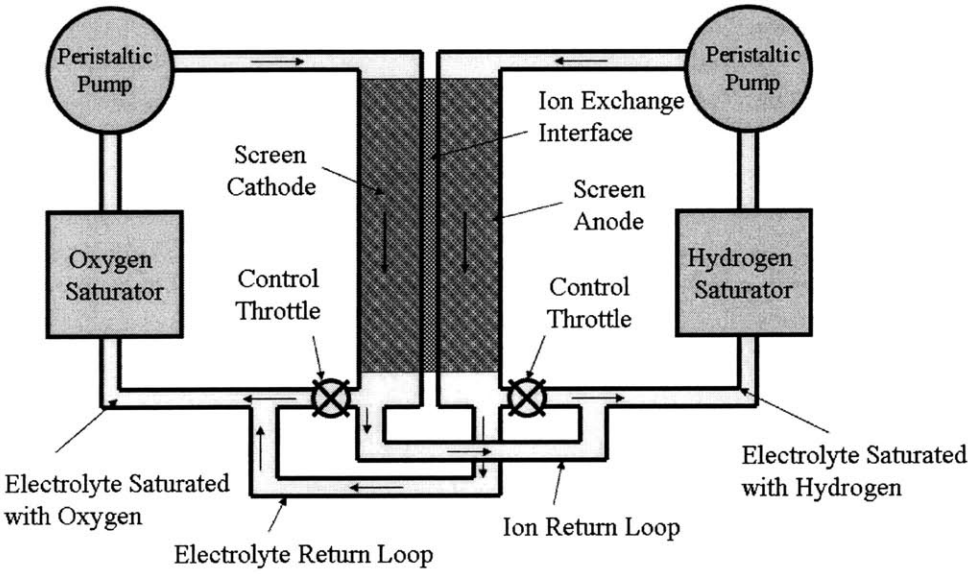

Figure 33: Fuel cell employing flooded electrodes and an ion return loop.

If concentration gradients existed, they would help carry current and aid in the mass transport. The migration of K^+ ions is beneficial in the well-mixed situation, but the best case scenario would be to have a concentration gradient as seen in a typical PGD electrode. The K^+ ions have a much harder time moving in the electrolyte compared to the smaller OH^- ions and are best left stationary. Thus, the "worst-case scenario" for the fuel cell system depicted in Figure 33 would be if the electrolyte were perfectly mixed.

The "worst-case scenario" can be modeled by assuming the concentration gradients are zero and that both ions move by migration alone. Equation (64) then gives

$$i = \frac{F^2 A}{RT}[D_- + D_+]C\frac{d\phi}{dx} \tag{76}$$

Solving for the potential distribution in the electrolyte

$$\phi = \phi_0 + \frac{i \cdot x}{\frac{F^2 A}{RT}[D_- + D_+]C} \tag{77}$$

We can solve for the magnitude of the desired volumetric flowrate in the ion return loop (and thus also in the electrolyte return loop) by substituting the expression for the potential gradient from equation (76) into equation (57) for the positive ion to yield,

$$J_+ = -\frac{i \cdot D_+}{FA[D_- + D_+]} + C_+ \vartheta \tag{78}$$

where the diffusion gradient term has been ignored. Equation (78) is just the molar flux of the positive ion in the well mixed electrolyte. Typically the velocity term would cancel out when calculating the current, or for simplicity the velocity term could just be considered zero. Then the molar flux is just equal to

$$J_+ = -\frac{i \cdot D_+}{FA[D_- + D_+]} \tag{79}$$

To solve for an estimate of the velocity of the K^+ ions migrating from the anode to the cathode in Figure 33, equation (79) is divided by the concentration to yield

$$\vartheta = \frac{i \cdot D_+}{FAC[D_- + D_+]} \tag{80}$$

Equation (80) thus gives a general estimate of the speed of migration of the positive ions from the anode to the cathode. For an electrolyte concentration of 1 Molar and a current density of 1 A/cm^2, the velocity according to equation (80) is 0.03 mm/s. The volumetric

flow rate in the ion return loop is thus small compared to the flow rate through the electrodes.

Equation (77) is plotted in Figure 34 over a distance of 1 mm at a constant current density of 1 A/cm^2 for the same values of the electrolyte concentration as given in Figure 32. Figure 35 is the same as Figure 34 except the distance has been increased to 10 mm. Figure 36 plots the overpotential required for various values of the current density over the same range of distances plotted in Figure 35, but at a constant concentration of 6 Molar.

From a comparison of Figure 34 to Figure 32, the potential drop across the gap increases as the cell becomes well mixed and the concentration gradient is removed. This is due to the K^+ ions being forced to migrate and carry a current. From Figures 35 and 36, it is clear that when the distances in the well-mixed cell become large, the ohmic overpotentials become large as well. However, unless the concentration is low, the current density is high, or the length between electrodes is long, the ohmic overpotential is not necessarily prohibitive. Though the potential drop in the well mixed cell with the ion return loop is slightly larger than in the cell with concentration gradients and no return loop, the benefit of the configuration in Figure 33 is that a current can be maintained across distances that would be prohibitive in a concentration gradient driven cell. The ion return loop removes the ion mass transport limitation.

Figures 35 and 36 still clearly illustrate that there are no scale-up advantages for fluidized bed electrodes and electrodes in general that rely on convection.

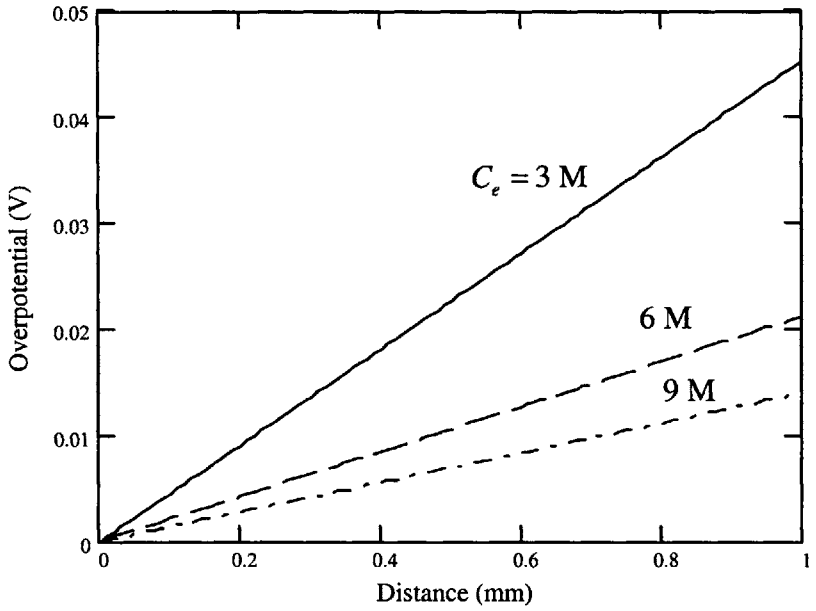

Figure 34: Overpotential required to conduct a current density of 1 A/cm^2 over a distance from 0 mm to 1 mm at several values of the electrolyte concentration.

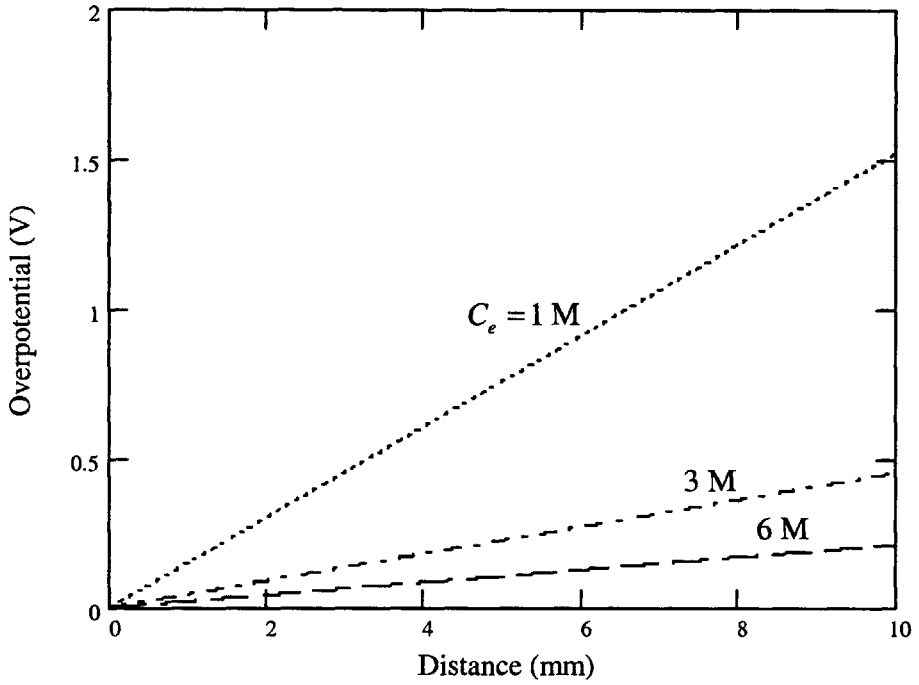

Figure 35: Overpotential required to conduct a current density of 1 A/cm^2 over a distance from 0 mm to 10 mm at several values of the electrolyte concentration.

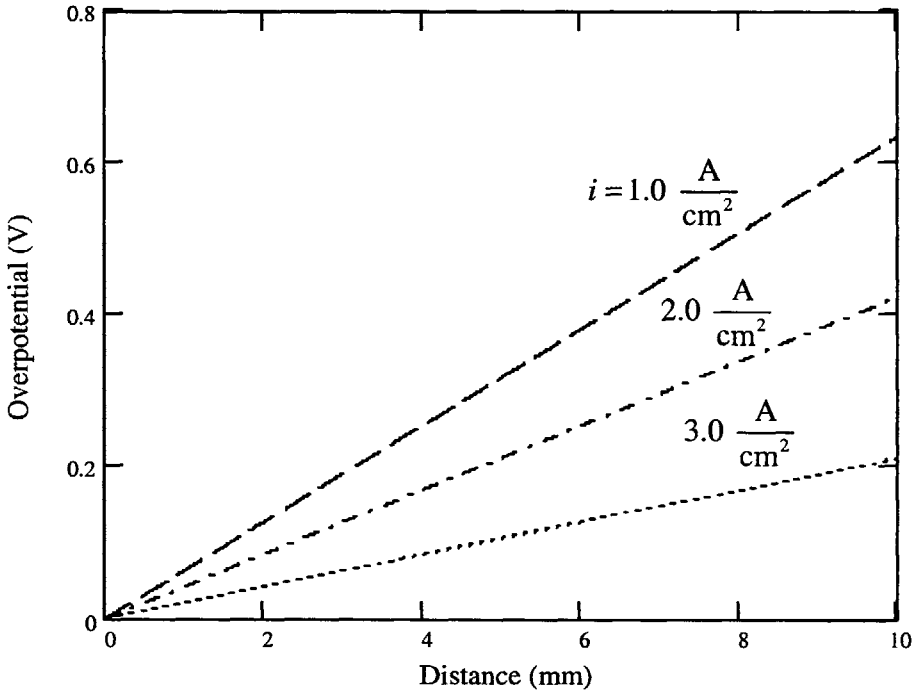

Figure 36: Overpotential required for various values of the current density for a range of distances; electrolyte concentration is constant at 6 Molar.

10.4 Influence of Electrolyte Concentration on the Limiting Current

It is clear from the previous plots that an electrolyte concentration of 1 Molar does not seem to have the ability to conduct the desired currents without creating significant overpotentials. Thus the electrolyte concentration will probably need to be increased, which is going to have a negative effect on both the saturation concentration and diffusion coefficient of oxygen in the electrolyte.

We can model the saturation concentration of oxygen in the electrolyte for a given electrolyte concentration using the correlations from reference [18]. The oxygen concentration depends on the partial pressure of oxygen according to Henry's law:

$$C_{o_2} = H_{o_2} P_{o_2} \tag{81}$$

Where P_{o_2} is the partial pressure of oxygen, and H_{o_2} is Henry's constant, which is given as [18]

$$H_{o_2} = \frac{x_{o_2}}{x_{o_2} - 1}\left(C_w + 2C_e\right) \tag{82}$$

where x_{o_2} is the mole fraction of the oxygen in the electrolyte, C_e is the concentration of the electrolyte, and C_w is the concentration of water.

C_w can be found by

$$C_w = \frac{1 - C_e v_e}{v_w} \tag{83}$$

where for KOH at 80 C, v_w is the partial molar volume of water, 17.9858 cm^3/mol, and v_e is the partial molar volume of the electrolyte, 18.8694 cm^3/mol [18].

The value of x_{o_2} can be found by solving [18]

$$\log\left(\frac{x_{o_2}^0}{x_{o_2}}\right) = k_{scx} C_e \tag{84}$$

where k_{scx} is the salting out coefficient and $x_{o_2}^0$ is the liquid phase mole fraction of oxygen in pure water. For KOH at 80 C, the values of k_{scx} and $x_{o_2}^0$ are 155 cm^3/mol and 1.440×10^{-5} respectively [18].

The oxygen diffusion coefficient at 80 C is given by [18]

$$D_{o_2} = 0.9188\times10^{-5} + 5.3940\times10^{-5}\exp\left(-262.6\cdot C_e\right) \tag{85}$$

where C_e is in mol/cm^3 and D_{o_2} is in cm^2/s.

The power output of the various flooded electrodes can be determined as a function of electrolyte concentration if the previous values of C_{o_2} and D_{o_2} used in the models are replaced by equations (81) and (85).

Figures 37 and 38 plot equations (81) and (85) for various values of the electrolyte concentration at a partial pressure of oxygen of 1 atm. Both Figures 37 and 38 indicate a strong dependence on the electrolyte concentration.

The performance of a screen electrode of 1 cm length is plotted in Figure 39 as a function of electrolyte velocity for various values of the concentration. The maximum power density in Figure 39 is higher than that in Figure 25 for a concentration of 1 Molar due to the temperature effect. Even though the concentration of oxygen decreases with temperature, the effect is outweighed by the increase in the diffusion coefficient of oxygen with temperature. The effect of increased electrolyte concentration in Figure 39, however, decreases both the oxygen saturation concentration and diffusion coefficient and thus performance as well.

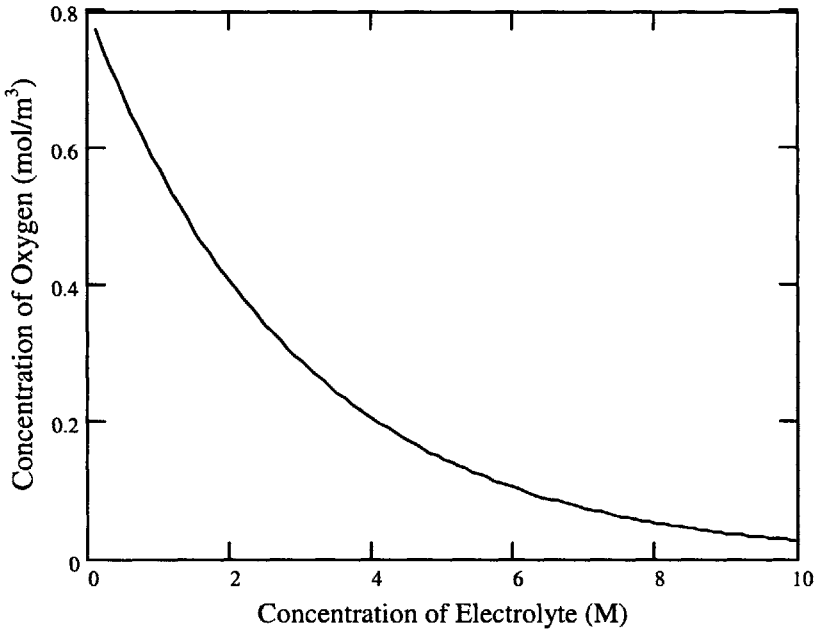

Figure 37: Influence of electrolyte concentration on saturation concentration of oxygen in the electrolyte at 80° C.

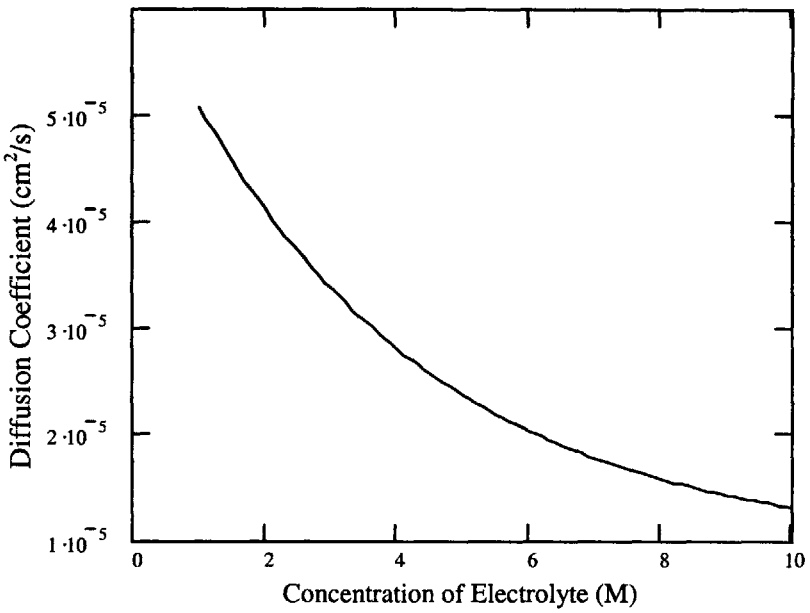

Figure 38: Influence of electrolyte concentration on the oxygen diffusion coefficient in the electrolyte at 80° C.

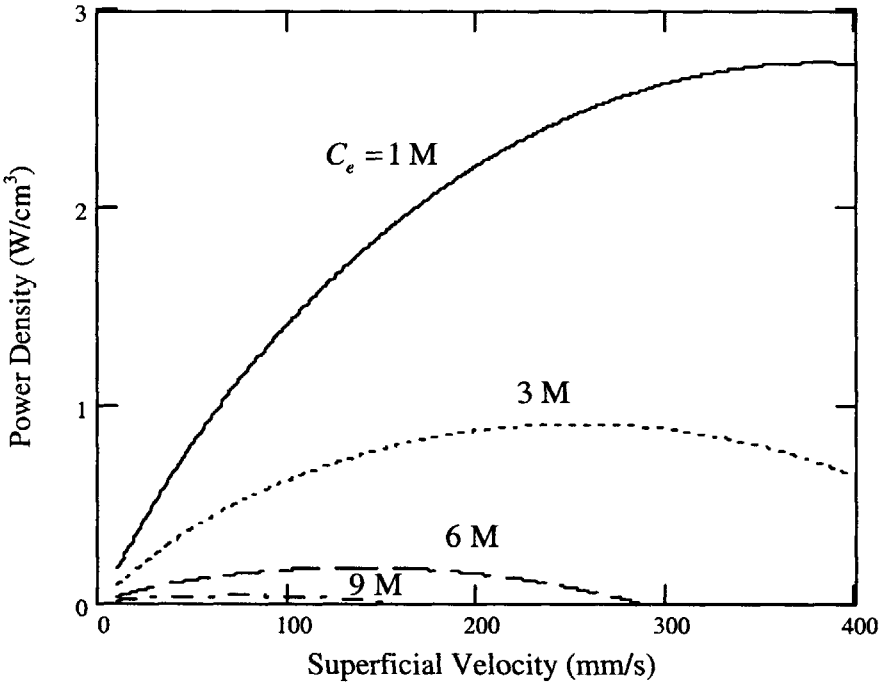

Figure 39: Net power density generated by a screen electrode 1 cm in length for various values of the concentration.

11.0 Final Conclusions and Recommendations for Further Work

A summary of the power per unit volume of the three flooded electrodes and the lowest value for the PGD electrode from Table 2 is given in Table 14. The power density of the packed bed electrodes depends on the diameter of the particles and the length of the bed (as shown in Figure 28); thus the data in Table 14 assume a length of 1 cm for all 3 flooded electrodes. The performance of all three flooded electrodes is less than the PGD electrode – even when the electrolyte concentration is only 1 Molar. The data of Section 10 show that if the electrolyte concentration is increased, performance decreases significantly. The data in Table 14 thus suggest that a flooded electrode using the typical electrolytes may not be capable of competing successfully with PGD electrodes. Note also that the data for the flooded electrodes represent upper limits to performance, while the data for the PGD electrode are lower bound on actual data.

The only electrode designs that could compete with PGD electrodes are very short and very thin packed beds of micrometer scale particles (or screens with similarly high area per unit volume). If the packed beds are made with even smaller particles and at correspondingly shorter lengths than those shown in Figure 28, then performance can be improved further. For instance, assume a 1 mm electrode length utilizing a particle of diameter 0.03 mm. The correlations for pressure drop and mass transfer are typically for larger beds and particle sizes, but the mass transfer coefficient in equation (35) is good to at least $Re \sim 3$. If we choose a velocity of 85 mm/s, which is near the optimum (and gives a Re of about 3), then assuming the pressure drop equation is valid, the achievable power density is about 8 W/cm^3. However, recharging the electrolyte flowing through these 1-D electrodes efficiently without taking up a lot of space for hardware would probably not be a trivial process. It remains to be seen if a feasible architecture can be created. Thus, unless a very unconventional design is used, the flooded electrodes are not competitive, at least not with a typical electrolyte. Section 11.2 does present a modified electrolyte that has the potential to increase the performance of flooded electrodes dramatically. Section 11.1 however first concludes the issue of fluidized bed electrodes.

Table 14: Power per Unit Volume of the PGD and Flooded Electrodes.

Electrode Type	PGD	FBE (1 M)	Packed Bed (1 M)	Packed Screen (1M)
Power (W/cm^3)	>4 (pure O_2)	0.35	>1.5	2.7

11.1 Fluidized Bed Electrodes

Conclusions of Presented Data and Models

From the provided analysis, the performance of the fluidized bed electrode is clearly inferior to the other electrode designs. All three claims mentioned at the beginning of this thesis regarding the performance of fluidized beds do not hold: mass transfer is not high compared to other electrode designs; the surface area is not particularly high per unit volume of the electrode; and the electrode has no scale-up advantages over any other electrode design. The mass transport is limited both by a supply limitation, due to not enough reactant being brought into the electrode, and a transport limitation, due to the product of the mass transfer coefficient and the surface area being too small. The surface

area cannot be increased by employing porous particles due to the relatively low mass transfer coefficient. The surface area can only be increased with smaller particles, which in turn require a lower velocity and thus increase the supply limitation. The required shape of the bed is still primarily two-dimensional, since ion transport limitations will be similar to those seen in fuel cells employing typical PGD electrodes. Just as with the other flooded electrodes, the ideal shape seems to actually be one-dimensional in nature; the power density increases as the bed height decreases to zero. The data in Section 5.3 seem to indicate that creating a three-phase bed would not improve performance.

The claims in Section 1.0 are likely expectations that have grown from the success of fluidized beds in chemical reactors. The expectation is that the benefits of fluidized beds in reactor designs will apply equally well to the use of fluidized beds in electrochemical reactors (electrodes); unfortunately, they do not.

Application of Magnetic Fields to Improve Performance

There is one other method available that may improve the performance of fluidized bed electrodes. Many studies have applied magnetic fields to fluidized bed reactors to improve performance. A thorough review of these magnetofluidized beds is given in reference [29]. Most of these studies have focused on gas-solid fluidized beds, but some have even studied liquid-solid and three-phase beds. Also, several studies have applied magnetic fields to electrochemical systems consisting of planar electrodes, as described in the review in reference [30]. However, we have been unable to find any studies to date that have applied magnetic fields to a fluidized bed used as an electrode. The application of magnetic fields has the potential to increase electrode output by increasing the mass transfer coefficient and the velocity through the bed, assuming the energy loss due to the power consumption of the solenoid is not significant. It has been found in gas-solid fluidized beds that gas throughputs of 20 times the minimum fluidization velocity can be achieved [29]. Fluidized beds exposed to AC fields in some cases have resulted in significant increases in the mass transfer coefficient. Even moderate increases in velocity and the mass transfer coefficient would improve performance enough that FBEs may become attractive on account of their other benefits.

Niche Applications

Certainly fluidized bed electrodes could still be advantageous in certain applications, especially if magnetic fields prove beneficial. For instance, the fact that the particles that compose the bed can be easily maintained and replaced may be of particular interest in biofuel cells, where the biological catalysts tend to break down after a short period of time. Granted, it may be just as easy to replace a packed bed as a fluidized bed. Also, if the biological catalyst is relatively cheap to make, then longer fluidized beds can be used without adding significant cost, assuming space is not a premium. However, without particular niche applications, or a significant improvement due to the application of magnetic fields, further consideration of fluidized bed electrode designs does not seem worthwhile.

11.2 Flooded Electrodes

The issue that affects all of the flooded electrode designs is the oxygen saturation limit of the electrolyte, as was discussed in Section 4.4. The electrolyte simply does not hold much oxygen. Equation (78) shows the oxygen concentration in the electrolyte could be increased by pressurizing the cell, but this tends to add cost and complexity to the design. Also, if a PGD electrode was pressurized in the same manner, its performance would still be better than that of the flooded electrode.

An alternative to increasing the oxygen concentration in the typical electrolyte by increasing the pressure is to instead modify the electrolyte to hold more oxygen.

Chemical Pressurization

The concept, first proposed at MIT by Omar Roushdy [31], is simple: since the electrolyte does not hold enough oxygen, cell performance could be enhanced by the addition of components to the electrolyte that act as oxygen carriers. In other words, the cell could be pressurized by chemical means.

The oxygen carriers initially explored by Rhoushdy were Perfluorocarbon (PFC) liquids. PFCs are an inert chemical with oxygen solubility over one-hundred times that of the typical electrolyte. Adding PFCs to the electrolyte has the potential to increase the oxygen concentration significantly. The primary advantage of a liquid emulsion composed of PFC and electrolyte is that very small PFC droplets are obtained which result in highly dispersed oxygen. In addition to the concentration improvement, the oxygen diffusion coefficient of these PFCs is also about 4 times that of pure water, which promises to further improve performance [32].

A second type of chemical pressurization would involve the entrainment of solid microparticles with high oxygen solubility in the electrolyte. Several solid materials have high oxygen carrying capacity. The advantage of the "microparticles" is that because they are solid, they have extremely low vapor pressures and thus should not evaporate in time, as do liquids. This is very advantageous especially compared to PFCs which are not environmentally friendly. PFCs are not a long-term solution for chemical pressurization. Microparticles can also be manipulated and filtered, which could be advantageous in particular electrode designs. Two of the many possible materials include silicone and Teflon AF. Silicone has the highest oxygen permeability rate of essentially any polymer. Teflon AF, produced by Compact Membrane Systems, is also known to have very high oxygen solubility.

If the PFC emulsions could successfully contribute even a fraction of the oxygen they are capable of carrying, the performance of the flooded electrodes could improve dramatically since current scales directly with concentration, and the mass transfer coefficient depends on the diffusion coefficient of oxygen in the electrolyte. Preliminary results of tests we have done on un-optimized PFC emulsions containing roughly 25% PFC by volume in a rotating disk electrode apparatus have shown nearly double the performance with the PFCs than without. Significant improvements beyond this are expected.

Consider the example of a screen electrode running on an emulsion of 50% PFC by volume. Assume the effective O_2 concentration in the emulsion is the average of the O_2 concentration in the electrolyte (which we just set to zero) and the O_2 concentration in the PFC. The PFC has an oxygen concentration of about 16 times that of the electrolyte in Table 5, so the emulsion's effective concentration is about 8 times that in Table 5. Assume the diffusion coefficient of oxygen in the emulsion is equal to the value in Table 5. Then the peak power density produced by a 1 cm screen electrode would be 22 W/cm^3, and the power produced by a 4 cm long electrode would be over 64 W per unit cross-sectional area, both at a velocity of around 725 mm/s. If the effective diffusion coefficient was instead twice the value listed in Table 5, the power density for the 1 cm electrode would be 36 W/cm^3 and the power produced by the 4 cm electrode would be 90 W per square centimeter, both at a velocity of about 850 mm/s. Thus chemical pressurization is one area worth further investigation.

Flooded Anodes and Carbon Fuels

Even without the consideration of chemical pressurization, there are certain applications where flooded electrodes may have advantages. Flooded electrodes offer the opportunity for researchers to take a more serious look at the use of carbon containing fuels in alkaline electrolyte fuel cells. Alkaline fuel cells have several advantages over other types in terms of kinetics and cost of materials. However, the alkaline fuel cell has one major obstacle: carbon dioxide is a potential poison to alkaline fuel cells. Even the carbon dioxide in air is a concern, which is why alkaline fuel cells have typically run on pure O_2. Recent studies [33] have shown that the carbon dioxide in air does not actually degrade the electrodes, as was originally thought. It still seems likely, however, that alkaline fuel cells running on carbon fuels would be problematic for the electrodes. The main concern in a PGD electrode is that the carbon dioxide produced as a product of the reacting fuel will then react with the electrolyte to form carbonate, which will then precipitate out of solution due to the high concentrations in the electrode pores where the fuel is reacting. The precipitated solid carbonate will then consequently clog the pores, which will choke mass transport and reduce the performance of the electrode.

In a fluidized bed electrode, however, and probably in flooded electrodes in general, "issues surrounding electrode poisoning due to formation of carbonate may be far less serious in [these designs] due to the elimination of the porous gas diffusion electrode" [3]. Without pores to clog, carbonate formation is no longer an issue. Since the electrolyte is easily circulated, directly filtering the electrolyte to remove the carbonate and replenish the hydroxyl ions would be possible. Thus carbon containing fuels can be used in alkaline fuel cells with fluidized bed electrodes. This is an important result. The authors in reference [34] found that alkaline solutions offer "faster kinetics both of the electro-oxidation of organic compounds and of oxygen reduction." Specifically, they measured peak current densities for a platinum disk. The peak current density of ethylene glycol was close to ten times higher in KOH than in acidic H_2SO_4. Several other alcohols were tested and gave similar results [34]. A lot of research is dedicated to liquid fuels due to their ability to greatly increase system power density. The reactivity of a rather complex liquid fuel however is usually very low in comparison to hydrogen in the acid

electrolytes and often chokes fuel cell performance. Thus the potentially higher reactivity of an alkaline fuel cell employing flooded electrodes and an appropriate alcohol fuel could be a major improvement, and is thus also worth further exploration.

References

1. J. Scholta, N. Berg, P. Wilde, L. Jorissen, and J. Garche, "Development and performance of a 10 KW PEMFC stack," J Power Sources, vol. 127, pp. 206-212, 2004.
2. I. Bar-On, R. Kirchain, R. Roth, "Technical cost analysis for PEM fuel cells," J. Power Sources, vol. 109, 71-75, 2002.
3. G.F. McLean., T. Niet, S. Prince-Richard, N. Djilali, "An assessment of alkaline fuel cell technology," Int. J Hydrogen Energy, vol. 27, pp. 507-526, 2002.
4. Y. Matsuno, A. Tsutsumi, K. Yoshida, "Improvement in electrode performance of three-phase fluidized-bed electrodes for an alkaline fuel cell cathode," Int. J. Hydrogen Energy, vol. 22, pp. 615-620, 1997.
5. J. Bockris, A. Reddy, Modern Electrochemistry, 2B, 2nd ed. New York, NY: Kluwer Academic/Plenum Publishers, 2000, pp. 1181-1184.
6. M. Eikerling, A.S. Ioselevich, A.A. Kornyshev, "How good are the electrodes we use in PEFC?" Fuel Cells, vol. 4, pp. 131-140, 2004.
7. Y. Matsuno, K. Suzawa, A. Tsutsumi, K. Yoshida, "Characteristics of three-phase fluidized-bed electrodes for an alkaline fuel cell cathode," Int. J. Hydrogen Energy, vol. 21, pp. 195-199, 1996.
8. E. Middelman, W. Kout, B. Vogelaar, J. Lenssen, E. de Waal, "Bipolar plates for PEM fuel cells," J. Power Sources, vol. 118, pp. 44-46, 2003.
9. A. Heinzel, F. Mahlendorf, O. Niemzig, C. Kreuz, "Injection moulded low cost bipolar plates for PEM fuel cells," J. Power Sources, vol. 131, pp. 35-40, 2004.
10. "Ballard Fuel Cell Power: Mark9 SSL," Online Brochure. Ballard Power Systems, Inc., 2004 <http://www.ballard.com/resources/documents/Mark 9 SSL.pdf>.
11. "Ballard Fuel Cell Power Module: Mark 902," Online Brochure. Ballard Power Systems, Inc., 2003 <http://www.ballard.com/resources/transportation/ Mark_902.pdf>.
12. "PowerStack MC250," Online Brochure. Astris Energi, Inc., September 2004 <http://www.astris.ca/PR/pdf/Astris-MC250.pdf>.
13. T. Berent, R. Mason, I. Fells, "Fluidised-bed fuel-cell electrodes," J. Applied Chem. Biotechnol., vol. 21, pp. 71-76, 1971.
14. M. Fleischmann, J.W. Oldfield, D.F. Porter, "Fluidised bed electrodes part 3. The cathodic reduction of oxygen on silver in a fluidised bed electrode," J. Electroanal. Chem., vol. 29, pp. 241-253, 1971.
15. H. Tanaka, N. Enoki, N. Kaneki, H. Sakai, K. Shimada, H. Hara, "A Three-Phase Fluidized Bed Fuel Cell," J. Electrochem. Soc., vol. 137, pp. 2798 -2800, 1990.
16. N. Epstein, "Liquids-Solids Fluidization," in Handbook of Fluidization and Fluid-Particle Systems, W. Yang, Ed. New York: Marcel Dekker, 2003, pp. 705–764.
17. L. Fan, Gas-Liquid-Solid Fluidization Engineering. Stoneham, MA: Butterworth Publishers, 1989, pp. 183-187.
18. J. Jo, S. Yi, "A computational simulation of an alkaline fuel cell," J. Power Sources, vol. 84, pp. 87-106, 1999.
19. I. Zaytsev and G. Aseyev, Eds., Properties of Aqueous Solutions of Electrolytes. Boca Raton: CRC Press, Inc., 1992, pp. 82-85, 227-230

20. W. Yang, "Particle Characterization and Dynamics," in Handbook of Fluidization and Fluid-Particle Systems, W. Yang, Ed. New York: Marcel Dekker, 2003, pp. 1-27.
21. A.F. Mills, Heat Transfer, 2nd ed. Upper Saddle River, NJ: Prentice Hall, Inc., 1999, pp. 355-362.
22. N. Wakao and S. Kaguei, Heat and Mass Transfer in Packed Beds. New York, NY: Gordon and Breach Science Publishers, Inc., 1982, pp. 154-156.
23. W. Yang, "Flow Through Fixed Beds," in Handbook of Fluidization and Fluid-Particle Systems, W. Yang, Ed. New York: Marcel Dekker, 2003, pp. 29-52.
24. U. Holeschovsky, J. Tester, W. Deen, "Flooded flow fuel cells: a different approach to fuel cell design," J. Power Sources, vol. 63, pp. 63-69, 1996.
25. "Stock Inventory: Platinum," Online Data, UNIQUE Wire Weaving Co. Inc., 2004 <http://www.uniquewire.com/metals/plat.cfm>.
26. I. Idelchik, Handbook of Hydraulic Resistance, 3rd ed. New York, NY: Begell House, Inc., 1996, pp. 522-524.
27. A.Bard, K. L. Faulkner, Electrochemical Methods: Fundamentals and Applications, 2nd ed. Hoboken, NJ: John Wiley and Sons, Inc., 2001, pp. 137-139.
28. J. Newman, K. Thomas-Alyea, Electrochemical Systems, 3rd ed. Hoboken, NJ: John Wiley and Sons, Inc., 2004, pp. 286-288.
29. Y. Liu, R. Hambly, R. Colberg, "Fundamental and practical developments of magnetofluidized beds: a review," Powder Technology, vol. 64, pp. 3-41, 1991.
30. R. Tacken, J. Janssen, "Applications of magnetoelectrolysis," J. Applied Electrochem., vol. 25, pp. 1-5, 1995.
31. O. Roushdy, "Flooded Fuel Cells," Ph.D. Thesis, Department of Mechanical Engineering, MIT, 2006.
32. L. Ju, J. Lee, W. Armiger, "Effect of the interfacial surfactant layer on oxygen transfer through the oil/water phase boundary in perfluorocarbon emulsions," Biotechnology and Bioengineering, vol. 37, pp. 505-511, 1991.
33. E. Gulzow, M. Schulze, "Long-term operation of AFC electrodes with CO_2 containing gases," J. Power Sources, vol. 127, pp. 243-251, 2004.
34. K. Matsuoka, Y. Iriyama, T. Abe, M. Matsuoka, Z. Ogumi, "Alkaline direct alcohol fuel cells using an anion exchange membrane," J. Power Sources, vol. 150, pp. 27-31, 2005.